

University of Windsor

Scholarship at UWindor

Electronic Theses and Dissertations

Theses, Dissertations, and Major Papers

1972

A study of the E.P.R. spectrum of the calcium(OH)₂:gadolinium(3+) system

Barry James Fox
University of Windsor

Follow this and additional works at: <https://scholar.uwindsor.ca/etd>

Recommended Citation

Fox, Barry James, "A study of the E.P.R. spectrum of the calcium(OH)₂:gadolinium(3+) system" (1972). *Electronic Theses and Dissertations*. 7993.
<https://scholar.uwindsor.ca/etd/7993>

This online database contains the full-text of PhD dissertations and Masters' theses of University of Windsor students from 1954 forward. These documents are made available for personal study and research purposes only, in accordance with the Canadian Copyright Act and the Creative Commons license—CC BY-NC-ND (Attribution, Non-Commercial, No Derivative Works). Under this license, works must always be attributed to the copyright holder (original author), cannot be used for any commercial purposes, and may not be altered. Any other use would require the permission of the copyright holder. Students may inquire about withdrawing their dissertation and/or thesis from this database. For additional inquiries, please contact the repository administrator via email (scholarship@uwindsor.ca) or by telephone at 519-253-3000ext. 3208.

A STUDY OF THE E.P.R. SPECTRUM OF THE

Ca(OH)₂ : Gd³⁺ SYSTEM

by

Barry James Fox

A Thesis

Submitted to the Faculty of Graduate Studies through the Department
of Physics in Partial Fulfillment of the Requirements for
the Degree of Master of Science at the
University of Windsor

Windsor, Ontario

1972

UMI Number: EC53114

INFORMATION TO USERS

The quality of this reproduction is dependent upon the quality of the copy submitted. Broken or indistinct print, colored or poor quality illustrations and photographs, print bleed-through, substandard margins, and improper alignment can adversely affect reproduction.

In the unlikely event that the author did not send a complete manuscript and there are missing pages, these will be noted. Also, if unauthorized copyright material had to be removed, a note will indicate the deletion.

UMI®

UMI Microform EC53114

Copyright 2009 by ProQuest LLC.

All rights reserved. This microform edition is protected against unauthorized copying under Title 17, United States Code.

ProQuest LLC
789 E. Eisenhower Parkway
PO Box 1346
Ann Arbor, MI 48106-1346

AAZ6353

APPROVED BY:

F. Mohr.

Hodgcock

RC Rumpfelt

391225

ABSTRACT

The system $\text{Ca}(\text{OH})_2 : \text{Gd}^{3+}$ was studied by electron paramagnetic resonance methods, to observe and measure ground state splitting in the Gd^{3+} ion ($^8S_{7/2}$). Fine structure was observed and the angular variation seemed consistent with a trigonal field.

The Spin Hamiltonian

$$H = \beta S \cdot g \cdot H + \sum_{n,m} B_{nm} T_{nm} \quad \begin{array}{l} n = 0, 2, 4, 6 \\ m = 0, 3, 6 \end{array}$$

was solved by an exact diagonalization process and the crystal field terms fitted using a multi-dimensional least squares method. The parameters were found to be

$$g_x = 1.990 \pm 0.005; \quad g_y = 1.991 \pm 0.005; \quad g_z = 1.989 \pm 0.006$$

In gauss

$$\begin{array}{lll} b_2^0 = -655.0; & b_4^0 = -11; & b_6^0 = +4 \\ b_4^3 = +27; & b_6^3 = -170; & b_6^6 = -0.06 \\ c_4^3 = +2; & c_6^3 = +124; & c_6^6 = -0.05 \end{array}$$

The fit had an R.M.S. error of 88 gauss for 63 lines.

It was postulated and is being tested at present that the B_{22} , B_{42} and B_{44} terms should be considered in the Hamiltonian. The intensity ratios were found to be 4 : 8 : 12 : 16 : 12 : 10 : 5.

The fit including orthorhombic terms had an R.M.S. error of 91 gauss and so offered no improvement. Terms that are non-linear in magnetic field are to be considered next, followed by hyperfine and nuclear Zeeman terms.

ACKNOWLEDGMENTS

The author wishes to thank Dr. F. Holuj for first suggesting this problem and for his guidance during the work. The assistance with the computer analysis so readily given by Dr. W. E. Baylis is gratefully acknowledged. Thanks are also due to Bob Wilson for his help with the experimental work and to my wife, Marilyn, for assistance in recording of data and preparation of diagrams.

TABLE OF CONTENTS

| | page |
|---|------|
| ABSTRACT | iii |
| ACKNOWLEDGEMENTS | v |
| LIST OF TABLES | viii |
| LIST OF FIGURES | ix |
| CHAPTER | |
| I. INTRODUCTION AND PURPOSE OF EXPERIMENT | 1 |
| II. CRYSTAL STRUCTURE OF $\text{Ca}(\text{OH})_2$ | 2 |
| III. THEORY | 5 |
| A. Electron Paramagnetic Resonance | 5 |
| B. The Trivalent Gadolinium Ion | 7 |
| C. The Complete Hamiltonian | 7 |
| D. The Spin Hamiltonian | 9 |
| E. The Spin Hamiltonian for Gd^{3+} | 9 |
| (1) Zeeman Term | 10 |
| (2) Crystal Field Term | 10 |
| (3) Tensor Operator Equivalents | 12 |
| F. Calculation of Matrix Elements | 15 |
| (1) Hamiltonian | 15 |
| (2) Derivative Hamiltonian | 17 |
| IV. INSTRUMENTATION | 20 |
| A. K-Band Spectrometer | 20 |
| (1) Klystron Stabilizer | 20 |
| (2) Microwave Circuit | 22 |
| (3) External Magnetic Field and Modulation | 23 |

| | page |
|---|------|
| B. Proton Magnetometer | 23 |
| V. EXPERIMENTAL PROCEDURE | 25 |
| A. X-Band | 25 |
| B. K-Band | 25 |
| (1) Crystal Orientation | 25 |
| (2) Angular Variation | 26 |
| (3) Measurement of Magnetic Field | 26 |
| (4) Measurement of Microwave Frequency | 28 |
| VI. DEVELOPMENT OF COMPUTER PROGRAMME | 29 |
| A. The Method | 29 |
| B. The Flow Chart | 34 |
| C. The Data Deck | 38 |
| D. Rate of Convergence | 40 |
| VII. RESULTS | 41 |
| VIII. DISCUSSION AND CONCLUSION | 52 |
| BIBLIOGRAPHY | 55 |
| APPENDIX A. Main Program | 57 |
| B. RTN 1 Main subroutine | 61 |
| C. CEIGEN: - Computes Eigenvalues and Eigen- vectors of a Hermitial Matrix (double precision complex) | 66 |
| D. STCM Similarity Transform Converts Matrix Elements to New Basis | 70 |
| E. DMINV Inverts a double precision matrix | 71 |
| F. DGMPRO Matrix Multiplication of two general double precision matrices | 74 |
| G. Calibration of Field across Magnet Gap | 75 |
| VITA AUCTORIS | 76 |

LIST OF TABLES

| | page |
|---|------|
| II.1 Structural Data for $\text{Ca}(\text{OH})_2$ | 4 |
| III.1 Some Spherical Harmonics expressed in Cartesian Co-ordinates | 12 |
| III.2 Relationship between Crystal Field Parameters including Normalization constant | 12 |
| III.3 Table of Tensor Operator Equivalents | 14 |
| III.4 Matrix Elements of Hamiltonian | 16 |
| III.5 Relationship between b_{nm} and B_{nm} | 17 |
| III.6 Values for Matrix Elements of the Tensor Operator Equivalents | 18 |
| III.7 Matrix Elements of Derivative Hamiltonian | 19 |
| V.1 Change in Frequency ranges for Resonators from X-band to K-band | 27 |
| VI.1 Example of Rate of Convergence | 40 |
| VII.1 Location Magnetic Axes | 41 |
| VII.2 Ratio of Line Intensities | 42 |
| VII.3 Proton Magnetometer Measurements of Resonant Fields | 44 |
| VII.4 Resonant Fields Converted to Kilogauss | 50 |
| VII.5 Calculated Values for Crystal Field Parameters | 51 |

LIST OF FIGURES

| | | page |
|-------|---|------|
| II.1 | Basal Projection of 3 Unit Cells for $\text{Ca}(\text{OH})_2$ | 3 |
| II.2 | Three Dimensional Representation of the $\text{Ca}(\text{OH})_2$ Unit Cell | 4 |
| III.1 | Block Diagram of K Band Spectrometer | 21 |
| V.1 | Resonator for Proton Magnetometer | 26 |
| VI.1 | Flow Chart for Computer Programme | 34 |
| VII.1 | Angular Variation in the XZ Plane (1010) | 44 |
| VII.2 | Angular Variation in the YZ Plane (1210) | 45 |
| VII.3 | Angular Variation in the XY Plane (0001) | 46 |
| VII.4 | Typical Spectrum with Field parallel to Z direction along 0001 axis | 47 |
| VII.5 | Typical Spectrum in direction perpendicular to Z | |
| | a) Along 1210 direction | |
| | b) Along 1010 direction | 48 |

CHAPTER I

INTRODUCTION AND PURPOSE OF EXPERIMENT

For S-state ions the resultant orbital angular momentum of the electrons is zero so that any degeneracy present in the state can only be due to spin. In such cases the ground state of the ion should not be split by the crystalline electric field. However, ground state splittings of S-state ions have been observed when the ions are placed in a crystalline environment.

The main purpose of this experiment was to observe and measure the ground state splittings produced when $Gd^{3+}(^8S_{7/2})$ was placed in the trigonal crystalline field of $Ca(OH)_2$ using the methods of Electron Paramagnetic Resonance Spectroscopy.

$Ca(OH)_2$ was chosen as the host crystal as it has a relatively simple structure and provides a substitution site with trigonal symmetry. The trivalent gadolinium ion was chosen as it is an S-state ion from the rare-earth group, and could be successfully introduced into the $Ca(OH)_2$ crystal.

Some of the previous work on the trivalent gadolinium ion in various site symmetries has been carried out by Low¹ (cubic), Jones, Baker and Pope² (rhombic), Serway and Marshall³ (trigonal), Buckmaster, Chatterjee and Shing⁴ (C_{3h} and C_3).

CHAPTER II

CRYSTAL STRUCTURE OF $\text{Ca}(\text{OH})_2$

X-ray studies have shown⁵⁻⁸ that $\text{Ca}(\text{OH})_2$ belongs to the hexagonal system, with space group $P(3,2/m,1)$, (CdI_2 type or D_{3d}^3). A projection of the structure is shown in Fig. II.1. Ca atoms lie in the invariant positions $(0,0,0)$, with point symmetry D_{3d} . O and H atoms lie in the special positions $\pm (1/3, 2/3, z_o)$ and $\pm (1/3, 2/3, z_h)$, respectively, both with point symmetry $3m$. Fig. II.1 shows 3 unit cells showing structure to 4th nearest neighbour and illustrating the relationship of the unit cell to the observed crystal habit. The outlined unit cell contains one molecule. The H positions were first postulated by Bernal and Megaw⁶. They have since been confirmed by x-ray diffraction⁸, neutron diffraction⁹, and nuclear magnetic resonance¹⁰.

The $\text{Ca}(\text{OH})_2$ structure consists of two sheets of hydroxyls lying in the (0001) plane. A sheet of Ca atoms is sandwiched between them. Each Ca atom is surrounded by six OH groups forming a slightly compressed octahedron. Fig. II.2 is a three dimensional representation of a unit cell illustrating these octahedra. Neutron diffraction studies revealed that the thermal motion of hydrogen is in the (0001) plane only^{9,11}. Consequently, there are no hydrogen bonds. The crystal is very soft (2 on Moh's scale) and has a perfect cleavage along (0001) . Structural data is given in Table II.1.

Single crystals of $\text{Ca}(\text{OH})_2$ were obtained by slow diffusion of NaOH and CaCl_2 in an aqueous solution free of CO_2 and O_2 . They were doped with Gd^{3+} during their growth.

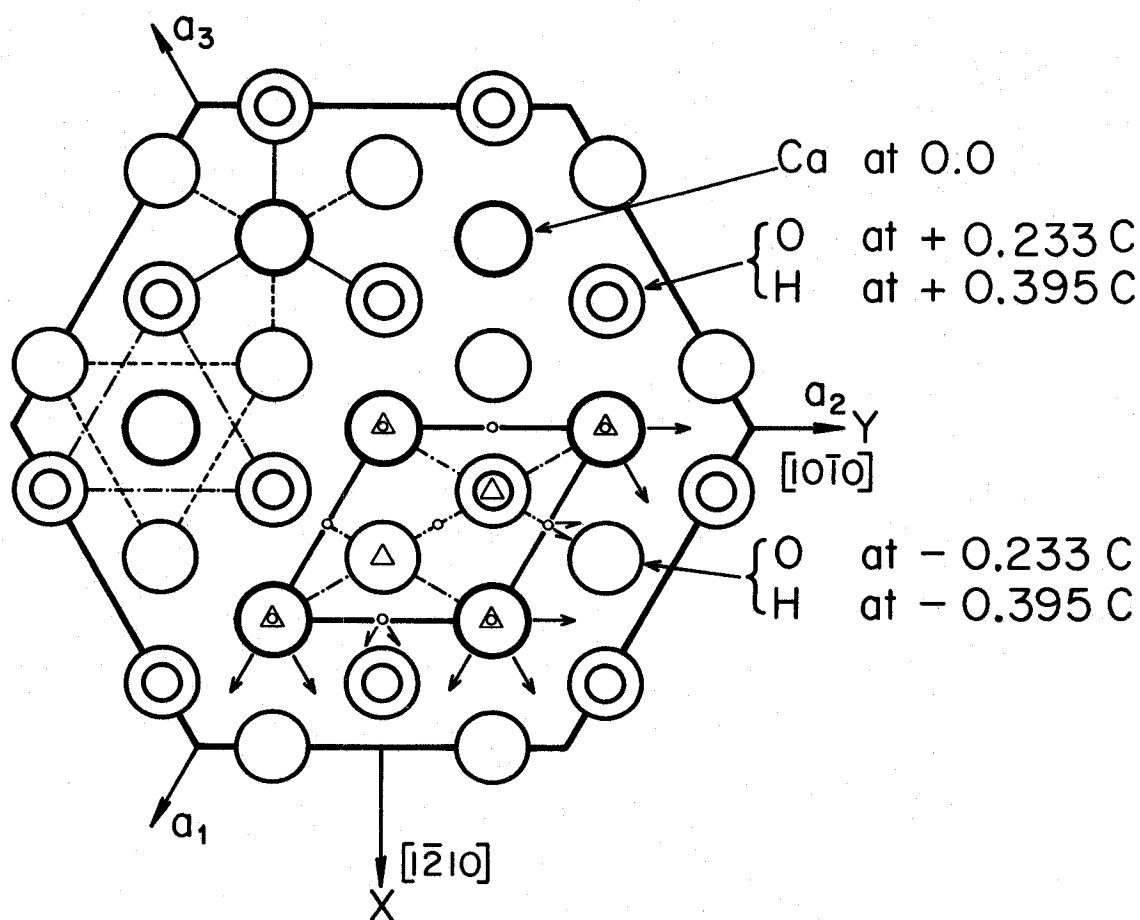


Fig. II 1 Structure of $\text{Ca}(\text{OH})_2$ projected on the (0001) plane. Some elements of the D_{3d}^3 space group are shown on the unit cell represented by the heavy outline.

- Δ 3-fold axis of rotation
- \circ inversion centre
- mirror plane
- \leftarrow horizontal 2-fold axis
- \leftarrow horizontal screw axis

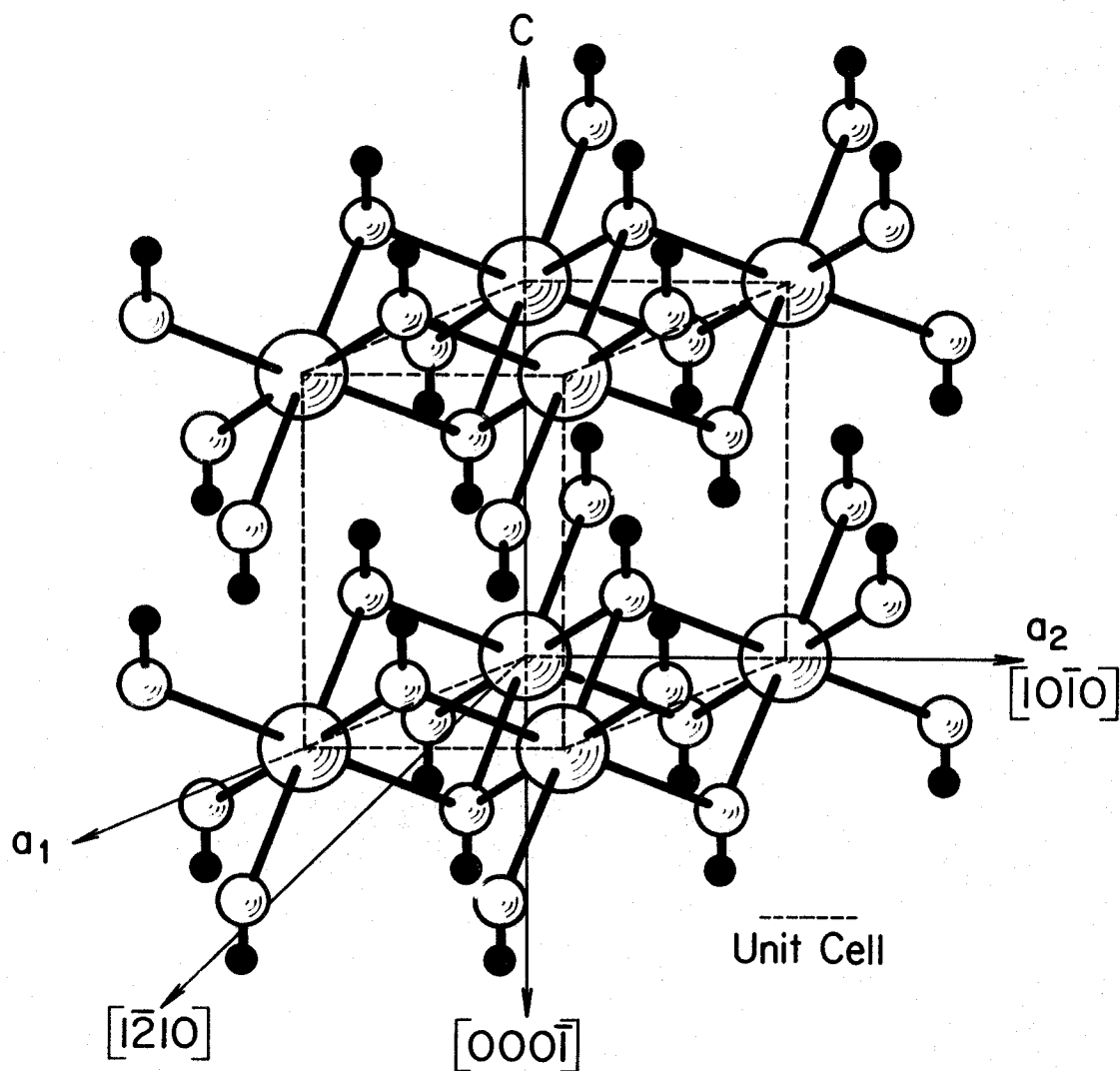


Fig. II.2 Three dimensional representation of unit cell of $\text{Ca}(\text{OH})_2$. The calcium ions appear at the corners of the unit cell, surrounded by an octahedron formed by the oxygen ions in planes above and below. The hydrogen ions (shaded) also lie in basal planes but further from the calcium ions.

TABLE II.1¹²

| | |
|---------------------------|----------------|
| Unit cell parameter a_0 | 3.5844 Å |
| Unit cell parameter c_0 | 4.8962 Å |
| Unit cell parameter z_0 | 0.2330 c_0 Å |
| Structure parameter z_h | 0.3950 c_0 Å |
| O-H separation | 2.6479 Å |

CHAPTER III

THEORY

A. Electron Paramagnetic Resonance

This phenomenon was first reported by Zavoyskiy(1945)¹³ and refers to the magnetic resonance of permanent magnetic dipole moments of electrons. It is shown in its simplest form by a set of non-interacting paramagnetic ions, each possessing a single unpaired electron and a 'spin only' magnetic dipole moment of $m_s g_s \beta$ ($m_s = 1/2$) where β is the Bohr magneton and $g_s = 2.00229$. In a steady magnetic field H , each dipole can orient itself parallel or antiparallel to H , with energies $-1/2 g_s \beta H$ and $+1/2 g_s \beta H$ (Zeeman splitting). Magnetic dipole transitions can be induced between these two energy levels by applying a high frequency magnetic field polarised perpendicular to H , and with frequency ν such that the quantum of high frequency energy equals the separation between levels, i.e.

$$h\nu = g_s \beta H \quad (\text{III.1})$$

There is then resonance absorption corresponding to the dipoles being flipped from the parallel to the antiparallel state and induced emission corresponding to the reverse process.

While the system remains in thermal equilibrium the population of the lower energy parallel state will exceed that of the antiparallel state, so a net absorption of high frequency power results. Saturation of

the system and its accompanying loss of absorption can occur when the rise in temperature caused by the absorption of energy results in an equalization of the two populations.

In the more general case for a free ion with a resultant angular momentum, $\underline{J} = \underline{L} + \underline{S}$ where \underline{L} and \underline{S} are the orbital and spin electronic angular momentum respectively. The energy levels are then given by

$$E = \pm Mg \beta H \quad (\text{III.2})$$

where g is the spectroscopic splitting factor and is defined by

$$g = 1 + \frac{J(J+1) + S(S+1) - L(L+1)}{2J(J+1)} \quad (\text{III.3})$$

and the Bohr magneton

$$\beta = \frac{eh}{4\pi mc} \quad (\text{III.4})$$

M is the projection of the electronic angular momentum J onto the magnetic field direction and so is the electronic magnetic quantum number. The use of M is necessary as the dipole is no longer aligned with, but instead precesses around, the magnetic field H . The frequency of precession is given by,

$$\omega = g \frac{e}{2mc} H \quad (\text{III.5})$$

for the energies to correspond to the photon energy

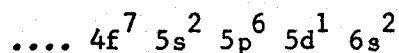
$$h\nu = g \beta H \quad (\text{III.6})$$

it can be seen that ΔM can only take the values $+1$ or -1 , so the selection rule governing allowed transitions is :

$$\Delta M = \pm 1 \quad (\text{III.7})$$

B. The Trivalent Gadolinium Ion

Gadolinium has the electronic structure



so that the trivalent gadolinium ion has a free ion ground state of $^8S_{7/2}$ in the $4f^7$ configuration. This indicates that the orbital angular momentum is $L=0$. Consequently, the energy levels will be 8-fold spin degenerate, splitting into 8 levels when the degeneracy is completely removed as would be expected for spin angular momentum $S = 7/2$.

C. The Complete Hamiltonian

For a paramagnetic ion in a crystalline field in the absence of a magnetic field, the complete Hamiltonian operator is

$$H = T + V_c + V_{so} + V_x + V_{ss} + V_{st} \quad (\text{III.8})$$

where

$$T = \sum_k (p_k^2 / 2m) \quad (\text{III.9})$$

is the total kinetic energy of the k th electron with momentum p_k and mass m where the sum is taken over all electrons for the ion.

The Coulomb term V_c consists of

$$V_c = - \sum_k \frac{Ze^2}{r_k} + \sum_{ij} \frac{e^2}{v_{ij}} \quad (\text{III.10})$$

The first term is the Coulomb attraction between the nucleus and the

electron summed over all electrons for the ion.

The V_{so} term is the potential energy due to spin-orbit coupling and is written

$$V_{so} = \sum_{ij} \lambda_{ij} \mathbf{l}_i \cdot \mathbf{s}_j \quad (\text{III.11})$$

where i and j are summed over all electron S . Assuming Russell-Saunders coupling, then

$$\sum_i \mathbf{l}_i = \mathbf{L} \quad \text{and} \quad \sum_j \mathbf{s}_j = \mathbf{S} \quad (\text{III.12})$$

so the term becomes

$$V_{so} = \lambda \mathbf{L} \cdot \mathbf{S} \quad (\text{III.13})$$

where λ is the spin-orbit coupling constant.

The term V_x represents the interaction between the paramagnetic ion with the crystal field potential

$$V_x = - \sum_k e_k \phi(\mathbf{r}_k) \quad (\text{III.14})$$

The term V_{ss} represents the magnetic dipole-dipole interaction between electrons and is written

$$V_{ss} = \sum_{jk} \frac{1}{r_{jk}^3} \left[\mathbf{s}_j \cdot \mathbf{s}_k - \frac{3 \mathbf{s}_j \cdot \mathbf{r}_{jk} \mathbf{r}_{jk} \cdot \mathbf{s}_k}{r_{jk}^2} \right] \quad (\text{III.15})$$

where the sum is extended over all pairs of electrons.

The term V_{s_1} represents the magnetic interaction between unpaired electrons and the nuclear magnetic moments (the hyperfine term.)

D. The Spin Hamiltonian

The complete Hamiltonian as written in (III.8) is very difficult to work with, a simpler treatment devised by Abragam and Pryce¹⁴ makes use of the spin Hamiltonian of the system. The actual spin of the system is replaced by the effective spin S where $(2S+1)$ is equal to the number of electronic levels in the ground state.

The general Hamiltonian is then written as

$$H = \beta \tilde{S} \cdot \tilde{g} \cdot \tilde{H} + \sum_{n,m} B_{nm} T_{nm} + \tilde{S} \cdot \tilde{A} \cdot \tilde{I} - g_N \beta_N \tilde{I} \cdot \tilde{H} \quad (\text{III.16})$$

where \tilde{g} and \tilde{A} are 2nd rank tensors. T_{nm} is a tensor operator equivalent and a function of the effective spin operator \tilde{S} . The B_{nm} are crystal field parameters.

The first term is the electronic Zeeman term and the g tensor now incorporates an anisotropic component due to the spin-orbit coupling. Zero field splitting is represented by the crystal field term $\sum_{n,m} B_{nm} T_{nm}$.

In the third term the A tensor describes the magnetic hyperfine interaction and also contains an anisotropic part due to dipolar coupling. The fourth term is the nuclear Zeeman term.

E. The Spin Hamiltonian for Gadolinium

As no hyperfine structure is observed for gadolinium at room temperature, the hyperfine term and the nuclear Zeeman term can be omitted so that the spin Hamiltonian for gadolinium can be written as

$$H = \beta \tilde{S} \cdot \tilde{g} \cdot \tilde{H} + \sum_{n,m} B_{nm} T_{nm} \quad (\text{III.17})$$

the terms of which are explained separately in the following paragraphs.

(1) Zeeman Term

Considering a frame of reference that diagonalises the g tensor, the Zeeman term can be written as

$$H = \beta (S_x \ S_y \ S_z) \cdot \begin{pmatrix} g_x & 0 & 0 \\ 0 & g_y & 0 \\ 0 & 0 & g_z \end{pmatrix} \cdot \begin{pmatrix} H_x \\ H_y \\ H_z \end{pmatrix}$$

$$H = \beta (g_x S_x H_x + g_y S_y H_y + g_z S_z H_z) \quad (\text{III.18})$$

$$H = \beta g_z H_z S_z + \beta/2 (h_+ S_- + h_- S_+)$$

where

$$h_+ = (g_x H_x + i g_y H_y); \quad h_- = (g_x H_x - i g_y H_y)$$

$$S_+ = (S_x + i S_y) \quad ; \quad S_- = (S_x - i S_y)$$

This can be written in terms of tensor operator equivalents T_{nm} . (See (III.26) and Table III.3)

$$H = \beta g_z H_z T_{10} + \beta \left(\frac{h_+}{\sqrt{2}} T_{1-1} - \frac{h_-}{\sqrt{2}} T_{11} \right) \quad (\text{III.19})$$

(2) Crystal Field Term

The crystal field term represented by $\sum_{n,m} B_{nm} T_{nm}$ is derived as follows. The Hamiltonian of the crystal field is given by

$$H_{cr} \equiv \sum_i -e V(x_i, y_i, z_i) \quad (\text{III.20})$$

where the crystal field potential V is a function of the position of the i th electron with the sum taken over all of the electrons in the unfilled shell. Assuming it satisfies Laplace's equation, V can be expanded in a series of spherical harmonics

$$V = \sum_i \sum_{n,m} A_{nm} r^n Y_{nm}(\theta_i, \phi_i) \quad (\text{III.21})$$

Many of the terms will have zero matrix elements and need not be considered.

(a) All terms $n > 6$ will have zero matrix elements. For f-electron wave functions the probability density $\psi^* \psi$ can be expanded in spherical harmonics only for $n \leq 6$ so matrix elements $n > 6$ vanish.

(b) Similarly all terms for which n is odd have zero elements. The probability density $\psi^* \psi$ is an even function while the potential is an odd function for odd n .

(c) The term containing $n = 0$ is an additive constant that is set to zero.

Further reductions can only be made by considering site symmetry. As the gadolinium ion is assumed to substitutionally replace the calcium ion it will be in a site of D_{3d} point symmetry so that the trigonal form of the crystal field potential must be used. This can be derived by considering the symmetry of the appropriate spherical harmonics $Y_{nm}(\theta, \phi)$ determined by the lowest value of m

| | | |
|-------------|-----------------|----------|
| $m = 0$ | Axial | |
| $m = \pm 2$ | 2 fold symmetry | |
| $m = \pm 3$ | 3 fold symmetry | |
| $m = \pm 4$ | 4 fold symmetry | (III.22) |
| $m = \pm 6$ | 6 fold symmetry | |

and by setting

$$A_{n0} r^n Y_{n0} = U_{n0}$$

and

$$\left[A_{nm} Y_{nm}(\theta, \phi) + A_{n(-m)} Y_{n(-m)}(\theta, \phi) \right] r^n = U_{n|m|}$$

then

$$V_{\text{trig.}} = U_{20} + U_{40} + U_{60} + U_{43} + U_{63} + U_{66} \quad (\text{III.23})$$

Expressing the spherical harmonics in cartesian co-ordinates

TABLE III.1

$$\begin{aligned} V_{20} &= 3z^2 - r^2 \\ V_{40} &= 35z^4 - 30r^2z^2 + 3r^4 \\ V_{60} &= 231z^6 - 315r^2z^4 + 105r^4z^2 - 5r^6 \\ V_{43} &= (x^2 - 3y^2)xz \\ V_{63} &= (11z^2 - 3r^2)(x^2 - 3y^2)xz \\ V_{66} &= x^6 - 15x^4y^2 + 15x^2y^4 - y^6 \end{aligned}$$

where

$$U_{nm} = D_{nm} V_{nm} \quad (\text{III.24})$$

A_{nm} and D_{nm} are related by the normalisation constants in Table III.2

TABLE III.2

$$\begin{aligned} D_{20} &= \frac{1}{4} \sqrt{\frac{5}{\pi}} A_{20} & D_{60} &= \frac{1}{32} \sqrt{\frac{13}{\pi}} A_{60} \\ D_{40} &= \frac{3}{16} \sqrt{\frac{3}{\pi}} A_{40} & D_{63} &= \frac{1}{16} \sqrt{\frac{13 \cdot 105}{\pi}} |A_{63}| \\ D_{43} &= \frac{3}{4} \sqrt{\frac{35}{\pi}} |A_{43}| & D_{66} &= \frac{1}{32} \sqrt{\frac{13 \cdot 21 \cdot 11}{\pi}} |A_{66}| \end{aligned}$$

V can be written in the form $f(r)P_{nm}(\theta, \phi)$ where $P_{nm}(\theta, \phi)$ are assoc. Legendre polynomials. Once V_{20} , V_{40} and V_{60} are known all even potentials up to sixth degree can be found by symmetry.

(3) Operator Equivalents

As gadolinium is an S state ion

$$\underline{L} = 0 \quad \text{then} \quad \underline{J} = \underline{S} \quad (\text{III.25})$$

so that the total angular momentum will be the spin angular momentum $J = \frac{7}{2}$.

Within the manifold of states for which $J = \frac{7}{2}$ matrix elements for the potential operators may be replaced by appropriate angular momentum operators.

This is achieved by everywhere replacing x, y and z by J_x, J_y, J_z with regard to the fact that J_x, J_y and J_z are non-commuting operators.

e.g.
$$xy \equiv \frac{1}{2} \alpha (J_x J_y + J_y J_x) \quad (\text{III.26})$$

where α is a multiplying constant so that

$$V_{20} = \alpha \bar{r}^2 [3J_z^2 - J(J+1)] \quad (\text{III.27})$$

This can be expressed as an angular momentum tensor operator T_{20} which has been normalised incorporating the $\alpha \bar{r}^2$ where

$$T_{20} = +\sqrt{\frac{1}{6}} \{3J_z^2 - J(J+1)\} \quad (\text{III.28})$$

The angular momentum operators have been tabulated by Buckmaster et al ¹⁷. The ones of importance in this Hamiltonian are listed in Table III.3. (see next page).

In this form the crystal field can be simply written as:

$$H_{cr} = \sum_{nm} B_{nm} T_{nm} \quad (\text{III.29})$$

$n = 2, 4, 6$

$m = 0, \pm 3, \pm 6$

The spin-Hamiltonian can then be written :

TABLE III.3

$$\begin{aligned}
T_{20} &= +\sqrt{\frac{1}{6}} \left[3J_z^2 - J(J+1) \right] \\
T_{40} &= +\frac{1}{2}\sqrt{\frac{1}{70}} \left[35J_z^4 - 5 \left(6J(J+1) - 5 \right) J_z^2 + \right. \\
&\quad \left. + 3 \left(J^2(J+1)^2 - 2J(J+1) \right) \right] \\
T_{4+3} &= \mp \frac{1}{2}\sqrt{\frac{1}{2}} \left[J_{\pm}^3 J_z + J_z J_{\pm}^3 \right] \\
T_{60} &= +\frac{1}{4}\sqrt{\frac{1}{231}} \left[231J_z^6 - 105 \left(3J(J+1) - 7 \right) J_z^4 + \right. \\
&\quad + 21 \left(5J^2(J+1)^2 - 25J(J+1) + 14 \right) J_z^2 \\
&\quad \left. - 5 \left(J^3(J+1)^3 - 8J^2(J+1)^2 + 12J(J+1) \right) \right] \\
T_{6+3} &= \mp \frac{1}{8}\sqrt{\frac{5}{11}} \left[J_{\pm}^3 + \left\{ 11J_z^2 - \left(3J(J+1) + 59 \right) J_z \right\} + \right. \\
&\quad \left. + \left\{ 11J_z^3 - \left(3J(J+1) + 59 \right) J_z \right\} J_{\pm}^3 \right] \\
T_{6+6} &= \frac{1}{8} J_{\pm}^6 \\
T_{1+1} &= \mp \sqrt{\frac{1}{2}} J_{\pm} \\
T_{10} &= + J_z
\end{aligned}$$

$$\begin{aligned}
H = & \beta g_z H_z T_{10} + \beta \left(\frac{h_+}{\sqrt{2}} T_{1-1} - \frac{h_-}{\sqrt{2}} T_{11} \right) + B_{20} T_{20} + B_{40} T_{40} \\
& + B_{60} T_{60} + (B_{43} + i C_{43}) T_{43} - (B_{43} - i C_{43}) T_{4-3} \\
& + (B_{63} + i C_{63}) T_{63} - (B_{63} - i C_{63}) T_{6-3} \\
& + (B_{66} + i C_{66}) T_{66} + (B_{66} - i C_{66}) T_{6-6} \quad \text{(III.30)}
\end{aligned}$$

F. Calculation of Matrix Elements

(1) The Hamiltonian

For a manifold of constant J with wave functions ψ_m (h_m is the z component of angular momentum), the elements in the secular matrix are the integrals

$$\int \psi_m^* \{T_{NM}\} \psi_{m'} d\tau \equiv \langle m | T_{NM} | m' \rangle \quad \text{(III.31)}$$

where T_{NM} transform as Y_N^M and vanish unless $m = m' + M$,

$$M = m - m'$$

(Proof by use of Wigner coefficients, Condon and Shortley, 1951²⁰).

Using this theorem it can be seen that as M can only take the values $0, \pm 1, \pm 3, \pm 6$, which establishes the non-zero matrix elements of the T_{NM} .

Using the tabulated numerical values for the matrix elements of the angular momentum Tensor Operators, the spin Hamiltonian matrix is set up as in Table III.4.

| $\langle +\frac{7}{2} \rangle$ | $\langle +\frac{5}{2} \rangle$ | $\langle +\frac{3}{2} \rangle$ | $\langle +\frac{1}{2} \rangle$ | $\langle -\frac{1}{2} \rangle$ | $\langle -\frac{3}{2} \rangle$ | $\langle -\frac{5}{2} \rangle$ | $\langle -\frac{7}{2} \rangle$ |
|---|--|--------------------------------|--|---|--|--|--|
| $\frac{7}{2} h_{11} + 7\sqrt{\frac{3}{2}} B_{20}$ $+ 3\sqrt{70} B_{40}$ $+ 15\sqrt{\frac{21}{11}} B_{60}$ | $+\frac{\sqrt{7}}{2} h_-$ | | $-6\sqrt{10}(B_{43} + iC_{43})$ $-180\sqrt{\frac{7}{11}}(B_{63} + iC_{63})$ | | | $90\sqrt{7}(B_{66} + iC_{66})$ | |
| $+\frac{\sqrt{7}}{2} h_+$ | $+\sqrt{3} h_-$ $\frac{5}{2} h_{11} + \sqrt{\frac{3}{2}} B_{20}$ $-39\sqrt{\frac{10}{7}} B_{40}$ $-75\sqrt{\frac{21}{11}} B_{60}$ | $+\sqrt{3} h_+$ | $+\frac{\sqrt{15}}{2} h_-$ | $-12\sqrt{10}(B_{43} + iC_{43})$ $+\frac{630}{\sqrt{11}}(B_{63} + iC_{63})$ | | | $90\sqrt{7}(B_{66} + iC_{66})$ |
| | $+\sqrt{3} h_+$ | $+\frac{\sqrt{15}}{2} h_+$ | $+\frac{\sqrt{15}}{2} h_-$ | $+2h_-$ | | | |
| $-6\sqrt{10}(B_{43} - iC_{43})$ $-180\sqrt{\frac{7}{11}}(B_{63} - iC_{63})$ | | | $\frac{1}{2} h_{11} - 5\sqrt{\frac{3}{2}} B_{20}$ $+ 27\sqrt{\frac{10}{7}} B_{40}$ $- 75\sqrt{\frac{21}{11}} B_{60}$ | | | $+\frac{\sqrt{15}}{2}(B_{43} + iC_{43})$ $-\frac{630}{\sqrt{11}}(B_{63} + iC_{63})$ | |
| | $+\sqrt{10}(B_{43} - iC_{43})$ $+\frac{630}{\sqrt{11}}(B_{63} - iC_{63})$ | | $+2h_+$ | $-\frac{1}{2} h_{11} - 5\sqrt{\frac{3}{2}} B_{20}$ $+ 27\sqrt{\frac{10}{7}} B_{40}$ $- 75\sqrt{\frac{21}{11}} B_{60}$ | $+\frac{\sqrt{15}}{2} h_-$ | | $+6\sqrt{10}(B_{43} + iC_{43})$ $+180\sqrt{\frac{7}{11}}(B_{63} + iC_{63})$ |
| | | | | $+\frac{\sqrt{15}}{2} h_+$ | $+\sqrt{3} h_+$ $-\frac{3}{2} h_{11} - 3\sqrt{\frac{3}{2}} B_{20}$ $- 9\sqrt{\frac{10}{7}} B_{40}$ $+ 135\sqrt{\frac{21}{11}} B_{60}$ | $+\sqrt{3} h_-$ | |
| | | | $+\frac{\sqrt{15}}{2}(B_{43} - iC_{43})$ $-\frac{630}{\sqrt{11}}(B_{63} - iC_{63})$ | | | | $+\frac{\sqrt{7}}{2} h_-$ |
| $90\sqrt{7}(B_{66} - iC_{66})$ | $90\sqrt{7}(B_{66} - iC_{66})$ | | | $+\sqrt{10}(B_{43} - iC_{43})$ $+180\sqrt{\frac{7}{11}}(B_{63} - iC_{63})$ | | | $-\frac{7}{2} h_{11} + 7\sqrt{\frac{3}{2}} B_{20}$ $+ 3\sqrt{70} B_{40}$ $+ 15\sqrt{\frac{21}{11}} B_{60}$ |

TABLE III.4.

Where the crystal field parameters are related to the conventional parameters b_n^m by :

TABLE III.5.

$$\begin{array}{lll}
 b_2^0 = \sqrt{\frac{3}{2}} B_{20} & b_4^0 = 3 \sqrt{\frac{10}{7}} B_{40} & b_6^0 = \frac{315}{\sqrt{231}} B_{60} \\
 b_4^3 = 15 \sqrt{2} B_{43} & b_6^3 = \frac{315}{2} \sqrt{\frac{5}{11}} B_{63} & b_6^6 = \frac{315}{2} B_{66}
 \end{array}$$

For computational ease the parameters are expressed in kilogauss, as $B_{nm}(\text{kg.}) = 0.0935 B_{nm}(\text{cm}^{-1})$.

The values of the matrix elements of the tensor operator equivalents used in the calculation of the Hamiltonian, for a manifold $J = \frac{7}{2}$ are given in Table III.6. (see next page).

(2) The Derivative Spin Hamiltonian

In the fitting process the matrix elements of the derivative Hamiltonian (DH) are required. The matrix elements of DH are the derivatives with respect to each parameter of the corresponding elements in the matrix H taken one at a time. Each matrix will consist of only one set of elements and their complex conjugates, for example the derivative matrix with respect to the parameter B_{43} will only contain elements parallel to the diagonal but in the 3 off diagonal position and its complex conjugate on the other side of the diagonal. So the matrix elements, the parameter and the off diagonal position can be represented as in Table III.7.

TABLE III.7

| | | |
|----------------------------------|-----------------------------------|---|
| $DH(GX) = -\frac{T_{11}}{2} H_x$ | $DH(GY) = i \frac{T_{11}}{2} H_y$ | 1 |
| $DH(GZ) = T_{10} H_z$ | $DH(B20) = T_{20}$ | 0 |
| $DH(B40) = T_{40}$ | $DH(B60) = T_{60}$ | |
| $DH(B43) = T_{43}$ | $DH(C43) = i T_{43}$ | 3 |
| $DH(B63) = T_{63}$ | $DH(C63) = i T_{63}$ | |
| $DH(B66) = T_{66}$ | $DH(C66) = i T_{66}$ | 6 |

TABLE III.6.

| | J | J _z | Matrix Element | | J | J _z | Matrix Element |
|--|-----|----------------|----------------|--|-----|----------------|----------------|
| T ₁₀ ^(7/2) | 7/2 | -7/2 | -3.500000D 00 | T ₂₀ ^(7/2) | 7/2 | -7/2 | 8.573214D 00 |
| | 7/2 | -5/2 | -2.500000D 00 | | 7/2 | -5/2 | 1.224745D 00 |
| | 7/2 | -3/2 | -1.500000D 00 | | 7/2 | -3/2 | -3.674235D 00 |
| | 7/2 | -1/2 | -5.000000D-01 | | 7/2 | -1/2 | -6.123724D 00 |
| | 7/2 | 1/2 | 5.000000D-01 | | 7/2 | 1/2 | -6.123724D 00 |
| | 7/2 | 3/2 | 1.500000D 00 | | 7/2 | 3/2 | -3.674235D 00 |
| | 7/2 | 5/2 | 2.500000D 00 | | 7/2 | 5/2 | 1.224745D 00 |
| | 7/2 | 7/2 | 3.500000D 00 | | 7/2 | 7/2 | 8.573214D 00 |
| T ₄₀ ^(7/2) | 7/2 | -7/2 | 2.509980D 01 | T ₆₀ ^(7/2) | 7/2 | -7/2 | 2.072548D 01 |
| | 7/2 | -5/2 | -4.661393D 01 | | 7/2 | -5/2 | -1.036274D 02 |
| | 7/2 | -3/2 | -1.075706D 01 | | 7/2 | -3/2 | 1.865293D 02 |
| | 7/2 | -1/2 | 3.227118D 01 | | 7/2 | -1/2 | -1.036274D 02 |
| | 7/2 | 1/2 | 3.227118D 01 | | 7/2 | 1/2 | -1.036274D 02 |
| | 7/2 | 3/2 | -1.075706D 01 | | 7/2 | 3/2 | 1.865293D 02 |
| | 7/2 | 5/2 | -4.661393D 01 | | 7/2 | 5/2 | -1.036274D 02 |
| | 7/2 | 7/2 | 2.509980D 01 | | 7/2 | 7/2 | 2.072548D 01 |
| T ₄₃ ^(7/2) and (-1)T ₄₋₃ ^(7/2) | 7/2 | -7/2 | 5.019960D 01 | T ₁₁ ^(7/2) and (-1)T ₁₋₁ ^(7/2) | 7/2 | -7/2 | -1.870829D 00 |
| | 7/2 | -5/2 | 3.794733D 01 | | 7/2 | -5/2 | -2.449490D 00 |
| | 7/2 | -3/2 | 0.0 | | 7/2 | -3/2 | -2.738613D 00 |
| | 7/2 | -1/2 | -3.794733D 01 | | 7/2 | -1/2 | -2.828427D 00 |
| | 7/2 | 1/2 | -5.019960D 01 | 7/2 | 1/2 | -2.738613D 00 | |
| | | | | 7/2 | 3/2 | -2.449490D 00 | |
| | | | | 7/2 | 5/2 | -1.870829D 00 | |
| T ₆₃ ^(7/2) and (-1)T ₆₋₃ ^(7/2) | 7/2 | -7/2 | 1.435904D 02 | T ₆₆ ^(7/2) and (-1)T ₆₋₆ ^(7/2) | 7/2 | -7/2 | 2.381176D 02 |
| | 7/2 | -5/2 | -1.899522D 02 | | 7/2 | -5/2 | 2.381176D 02 |
| | 7/2 | -3/2 | 0.0 | | | | |
| | 7/2 | -1/2 | 1.899522D 02 | | | | |
| | 7/2 | 1/2 | -1.435904D 02 | | | | |

J_z represents the initial state of T_{nm}^(7/2) and the final state for T_{n-m}^(7/2)

CHAPTER IV

INSTRUMENTATION

A. K-Band Spectrometer

The k-band spectrometer was of balanced bridge design, using a circulator, with the microwave frequency stabilized against the sample cavity. A block diagram of the system is shown in Fig. IV 1. The microwave power was supplied by a Varian model VA 98M reflex klystron producing 30 milliwatts of power.

(1) Klystron Stabilizer

The klystron frequency was stabilized to the cavity resonant frequency using a Teltronic Model KSLP Klystron Stabilizer. The stabilizer works on the principle of automatic-frequency control (A.F.C.). A sine wave modulation of approximately 70 KHz was impressed on the reflector voltage, thus causing a small amount of frequency modulation. If the klystron frequency is tuned at or near the cavity resonant frequency, the output detected by the A.F.C. detector will contain a 70 KHz component. The A.F.C. signal is amplified and then applied to the phase sensitive detector (P.S.D.), built into the stabilizer, which compares the signal with the original modulation signal. The result is a D.C. error voltage with a polarity and magnitude proportional to the difference between the klystron oscillator frequency and the resonant frequency of the cavity. The error voltage is applied to the reflector of the klystron in such a manner that the klystron frequency is pulled back to the frequency of the cavity.

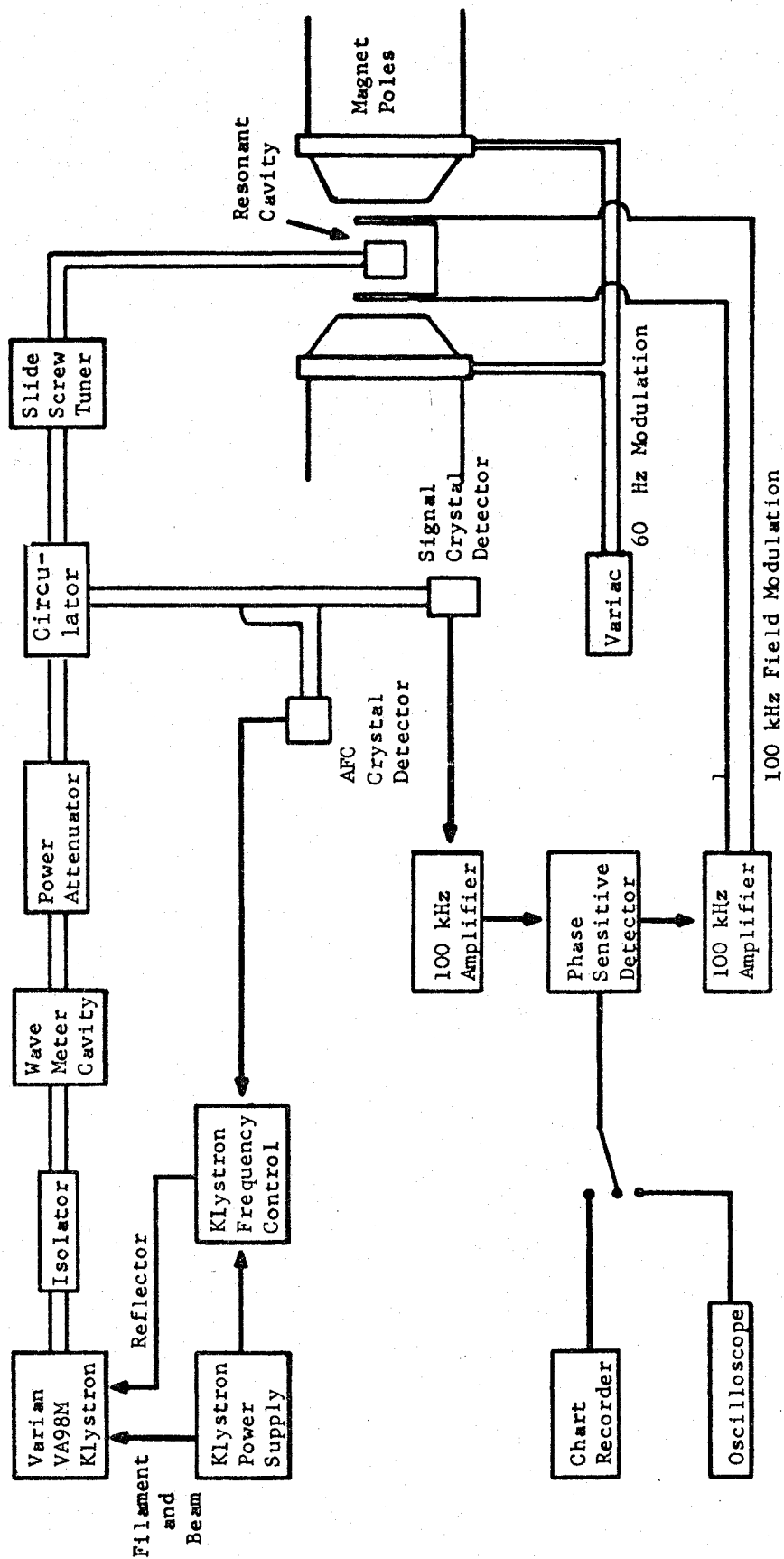


FIG. IV.1. BLOCK DIAGRAM OF K BAND SPECTROMETER

(2) Microwave Circuit

Microwaves are prevented from re-entering the klystron by use of an isolator, which is a two-terminal pair microwave ferrite device which makes use of the Faraday effect to permit transmission of microwaves in one direction and prevents their transmission in the opposite direction. A tuneable cylindrical cavity is used as a wavemeter, and an attenuator is used to control the power reaching the sample cavity which may be necessary in cases of saturation.

A three port circulator is used to allow transmission of klystron power to the cavity and power reflected at resonance from the cavity to the detector, without power going directly to the detector or any reflected power returning to the klystron arm. The cavity arm can be matched to the klystron arm by means of a slide-screw tuner. An E.P.R. absorption in the cavity then causes a mismatch, so that power is reflected from the cavity into the detector arm. In practice the cavity is slightly mismatched in order to allow sufficient power to bias the detector crystal.

The magnetic resonant absorption signal is detected by the crystal detector. The resonant signal is pre-amplified and then fed into the Princeton Applied Research (P.A.R.) model JB-6 Lock-in Amplifier, which compares the phase and frequency of the resonant signal with the original 100 KHz modulation signal in a similar way to the P.S.D. (previously described) of the A.F.C. The result is a derivative signal proportional to the resonant signal, which can be displayed on the oscilloscope or chart recorder as a function of magnetic field. To allow display on the oscilloscope the magnetic field is modulated at 60 Hz with a 'Variac', in addition to the 100 KHz. The horizontal sweep of the oscilloscope is

connected to a 60 H_z source and synchronised with the modulation using a phase shifter. The method of oscilloscope display allows one to observe E.P.R. signals when both the magnetic field and crystal orientation are varied. As such it provides a rapid means of studying angular variation.

The cylindrical cavity used is of glass having the inside surface sputtered with gold. Operating in the TE₀₁₁ mode the cavity has been successfully used in this laboratory prior to this. Incorporated with the cavity is a rotating mechanism previously developed in this laboratory²¹. It allows rotation of the crystal about a horizontal axis which when combined with rotation of the magnet about a vertical axis means any crystal orientation can be reached for anisotropy studies.

(3) External Magnetic Field and Modulation

The external magnetic field is produced by a 12 inch Varian electromagnet with a 3.5 inch gap and rotating base. The magnet is stabilized by a Fieldial model V-FR 2503 (Varian) control unit, which keeps the field value constant to within one Gauss for several hours. It is possible to get a linear field sweep up to 20 KGauss.

Magnetic field modulation at 100 KH_z is generated by an oscillator built into the P.A.R. Lock-in amplifier. This signal is amplified externally and applied to two Helmholtz coils connected in series and mounted on either side of the cavity.

B. Proton Magnetometer

Measurements of magnetic field strength are obtained by means of a proton magnetic resonance oscillator method using an external marginal oscillator, tuning circuit and amplifier, together with a wide band amplifier

and electronic counter, Hewlett-Packard No. 5253. Several complementary probes using rubber as a proton source have been constructed in order to cover the wide frequency range required.

CHAPTER V

EXPERIMENTAL PROCEDURE

A. X-Band

Ca(OH)_2 crystals doped with Gd^{3+} were investigated using an X-band spectrometer. Preliminary work indicated small signals whose intensity decreased as the field moved from the crystal axes. The impossibility of obtaining a complete angular variation made it necessary to move to K-band for the increased sensitivity.

B. K-Band

(1) Crystal Orientation

The symmetry of the crystal habit together with perfect cleavage in the basal plane allowed the crystallographic axes to be determined visually within 2° . The crystal was glued with the pin parallel to c-axis $[0001]$ as the tabular nature of the crystal caused the cavity resonance to move outside the klystron range as the crystal rotated for any other mounting.

The magnetic axes of the crystal were determined searching orientations that represented simultaneous turning points of the resonance lines for rotation of the magnet and the crystal. These orientations were plotted on a Wulffnet to check that they were mutually perpendicular.

The relationship of the axis of crystal rotation to that of the magnet rotation was checked. A determination was made of the collapse point of a pair of lines on the positive side of the magnet, with the field strength constant the crystal was rotated through exactly 180° and the

collapse point of the same pair of lines searched for on the negative side of the magnet. The midpoint of the two magnet orientations was the axis of crystal rotation. As a result all readings on the magnet scale had to be corrected by -1.4° before plotting on the Wulff net.

(2) Angular Variation

From the positions of the three axes the planes perpendicular to each axis but containing the other two axes were plotted. An angular variation was carried out with a 10° interval for the magnetic field direction moving in each of these planes in turn, $XY(0001)$, $XZ(1\bar{2}10)$ and $YZ(10\bar{1}0)$.

(3) Measurement of Magnetic Field

In order to use the proton magnetometer for magnetic field strength measurements a new set of probes had to be constructed to extend the upper limit of measurement from 30 MHz to the 53 MHz frequency of the high field resonance line. As the coaxial cable from the oscillator to the probe formed part of the tuning circuit it was possible to increase the frequency by shortening the cable and reducing the number turns in the inductor enclosing the proton source (rubber). The frequency was increased to 60 MHz but the intensity of the proton signal became too low to work with.

A satisfactory signal intensity and frequency range was obtained by decreasing the capacitance of the cable by using a grounded brass tube as shielding with the current carried to the inductor by two stiff wires separated from each other and the shielding by spacers set at intervals along the tube, (see Fig. V.1). The change of range of X-band resonators using this probe is given in Table V.1.

TABLE V.1

| Resonator Number | Range | |
|---------------------|--------------------|--------------------|
| | X-Band Unit MHz | K-Band Unit MHz |
| 5 | 10.8 - 16.1 | 13.1 - 22.5 |
| 6 | 14.5 - 21.7 | 18.7 - 32.0 |
| 7 | 20.0 - 30.0 | 31.4 - 56.3 |
| 8 | | 34.5 - 61.5 |

Actual measurements were made using a double beam oscilloscope. The crystal rotator and magnet scale were set at the required orientation. Each E.P.R. line in turn was centred on one of the oscilloscope beams, using the second beam the P.M.R. line was tuned to the E.P.R. line. The frequency of oscillation was then read from the digital output of the electronic counter. This frequency can be converted to magnetic field strength using the relation

$$h\nu = g_P \beta_N H$$

$$H = \frac{h}{g_P \beta_N} \nu \quad (V.1)$$

$$H(\text{KGauss}) = 0.234869 \nu(\text{MHz})$$

where H is magnetic field strength
 h is Planck's constant

g_p is the proton g value
 β_N is the nuclear magneton
 ν is the frequency of oscillation.

The accuracy of positioning the least intense E.P.R. lines was improved by using the chart recorder. With the field value set close to resonance, the field was swept over 50 gauss tracing the line on the chart thus allowing the exact centre to be marked and the field backed up to that point using the incremental field setting. The method was checked using the DPPH marker line and there was no loss in accuracy compared to a visual method.

(4) Measurement of Microwave Frequency

A small amount of the free radical α, α' -diphenyl- β -picryl hydrazyl was included with the sample to act as a marker to measure the microwave frequency using the relation

$$\begin{aligned}
 h\nu &= g_D \beta H_D \\
 \nu &= \frac{g_D \beta}{h} H_D
 \end{aligned}
 \tag{V.2}$$

where ν is the microwave frequency
 g_D is DPPH g value = 2.0036
 H_D is the field value of the DPPH resonance.

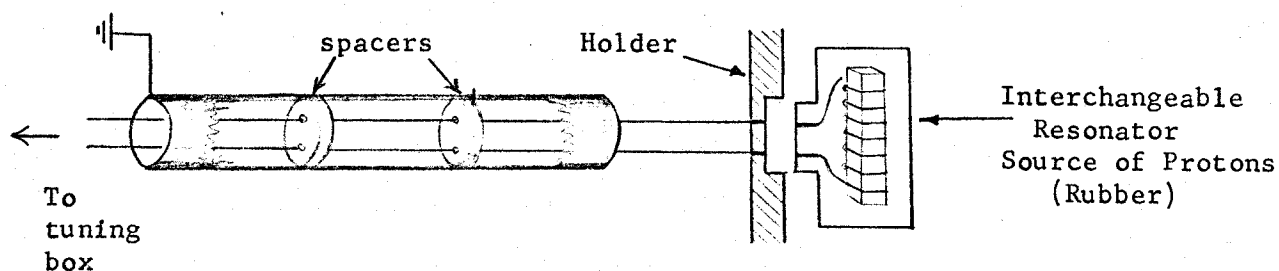


Fig. V.1.

CHAPTER VI

DEVELOPMENT OF COMPUTER PROGRAMME

A. The Method

The computer analysis was first attempted using a method for exact diagonalization of the generalized spin-Hamiltonian based on a program obtained from Buckmaster et al.¹⁹. However the necessity of measurements at two frequencies for each orientation made the program unsatisfactory for use in temperature dependence studies to follow.

A method of parameter fitting using multi-dimensional Newton-Raphson Least-Squares Minimization developed by Dr. W.E. Baylis was used so that the program could be generalized. This enabled it to accept data at any orientation and to fit a curve using data from different orientations rather than different frequencies.

The one dimensional Newton-Raphson Method²² is obtained analytically from following condition on the Taylor's series expansion.

$$f(\chi_n + h) = f(\chi_n) + h.f'(\chi_n) + \frac{h^2}{2!} f''(\chi_n) + \dots = 0 \quad (\text{VI.1})$$

where χ_n is an approximation of the root of the equation. This can be written in partial derivative form as:

$$\frac{\partial}{\partial \chi_n} f(\chi_n + h) = \frac{\partial}{\partial \chi_n} f(\chi_n) + h \cdot \frac{\partial}{\partial \chi_n} f'(\chi_n) + \dots = 0 \quad (\text{VI.2})$$

The problem of fitting the experimental data can be overcome in the following way. The Hamiltonian can be expressed as a function of a number of fitting parameters p_i ($i = 1, 2, \dots, I_{\max}$), the experimentally measured magnetic field values B , and other experimental parameters necessary

such as orientation \hat{k} or temperature T. B is a function of orientation so that the resonant fields occur as (N-1) values for each of M orientations where N will represent the degeneracy of the ground state. So the Hamiltonian can be expressed as

$$H = (p_1, p_2, \dots, p_{\max}, B, \hat{k}, T, \dots) \quad (\text{VI.3})$$

The Hamiltonian is represented in an n-dimensional basis $\{|\alpha\rangle\}$. The matrix elements for the Hamiltonian and its first and second derivatives with respect to the parameters must be known or able to be calculated

$$\langle \alpha | H | \beta \rangle \quad (\text{VI.4})$$

$$\langle \alpha | \partial H / \partial p_i | \beta \rangle \quad (\text{VI.5})$$

$$\langle \alpha | \partial^2 H / \partial p_i \partial p_j | \beta \rangle \quad (\text{VI.6})$$

The matrix elements of (VI.4) are given in Table III.4 while those for (VI.5) are given in Table III.6. As the parameters occur linearly in the Hamiltonian with no cross products the elements of (VI.6) will be zero.

For each set of external parameters (B, \hat{k}, T, \dots) (in this case for M(N-1) resonant field values), the Hamiltonian is diagonalized using the subroutine CEIGEN (see appendix). The subroutine is basically an extension of the Jacobi method to Hermitean matrices^{23,24} and is double precision, complex.

A new set of basis vectors $\{|i\rangle\}$, (in terms of the original set $\{|\alpha\rangle\}$, $|i\rangle = \sum_{\alpha} |\alpha\rangle \langle \alpha | i \rangle$) is then obtained in which the Hamiltonian is diagonal

$$\langle i | H | j \rangle = \delta_{ij} E_i \quad (\text{VI.7})$$

The difference between one adjacent pair of eigenenergies ($E_{k_1} - E_{k_2}$) will correspond to the transition energy experimentally determined from measurement of the microwave frequency ν_k . The correspondence between the pair of eigenenergies chosen and the resonant field representing that transition must be known. In this case the correspondence was determined and the programming simplified by taking all measurements at orientations where the resonant lines were separated and in order.

A least squares sum is formed from:

$$\{(E_{k_1} - E_{k_2}) - \nu_k\}^2 \quad (\text{VI.8})$$

$$= \{(E_{k_1} - E_{k_2}) - \frac{g_D H_D}{g_s}\}^2 \quad (\text{VI.9})$$

where the transition energy in (VI.9) is expressed in units of gauss and is determined from the resonant field of the DPPH(H_D). The value of the least squares sum f is then determined by summing over the total number of transitions measured $(N-1)M$ and dividing by the number of degrees of freedom (N free = number of transitions - number of parameters).

The multi dimensional Newton-Raphson method finds the value of $\underline{p} = (p_1, p_2, \dots, p_i)$, representing a vector in i -dimensional space where i is the number of parameters, such that $\frac{\partial f}{\partial p_i}(\underline{p}) = 0$ by solving iteratively the equation for the displacement $\underline{\delta}$ is

$$\frac{\partial}{\partial p_i} f(\underline{p} + \underline{\delta}) \approx \frac{\partial}{\partial p_i} f(\underline{p}) + \sum_j \frac{\partial^2}{\partial p_i \partial p_j} f(\underline{p}) \delta_j = 0 \quad (\text{VI.10})$$

The solution is:

$$\delta_i = - \sum_j M_{ij} \frac{\partial}{\partial p_j} f(\underline{p}) \quad (\text{VI.11})$$

where $((M_{ij}))$ is the inverse of $((\frac{\partial^2}{\partial p_i \partial p_j} f(\underline{p})))$
and

$$\sum_j M_{ij} \frac{\partial^2}{\partial p_j \partial p_i} f(\underline{p}) = \delta_{ii},$$

The inversion is carried out by the subroutine DMINV (see appendix).
The value of δ_i is then added to p_i to give the new estimate of the parameter.

The first and second derivatives of the least squares sum f required in the calculation are determined using perturbation theory.

$$\begin{aligned} \frac{\partial f}{\partial p_i} &= \frac{\partial}{\partial p_i} \frac{\sum_k \{ (E_{k1} - E_{k2}) - \frac{g_D H_D}{g_s} \}^2}{N_{free}} \\ &= 2 \sum_k \left(\frac{\partial E_{k1}}{\partial p_i} - \frac{\partial E_{k2}}{\partial p_i} \right) \frac{\{ (E_{k1} - E_{k2}) - \frac{g_D H_D}{g_s} \}}{N_{free}} \end{aligned} \quad (VI.12)$$

and

$$\begin{aligned} \frac{\partial^2 f}{\partial p_i \partial p_j} &= 2 \sum_k \left\{ \left(\frac{\partial E_{k1}}{\partial p_i} - \frac{\partial E_{k2}}{\partial p_i} \right) \left(\frac{\partial E_{k1}}{\partial p_j} - \frac{\partial E_{k2}}{\partial p_j} \right) \right. \\ &\quad \left. - \left(\frac{\partial^2 E_{k1}}{\partial p_i \partial p_j} - \frac{\partial^2 E_{k2}}{\partial p_i \partial p_j} \right) \frac{\{ (E_{k1} - E_{k2}) - \frac{g_D H_D}{g_s} \}}{N_{free}} \right\} \end{aligned} \quad (VI.13)$$

where

$$\frac{\partial E_k}{\partial p_i} = \lim_{\delta_i \rightarrow 0} \left\{ E_k(\underline{p} + \delta_i \hat{i}) - E_k(\underline{p}) \right\} \quad (VI.14)$$

where \hat{i} is a unit vector in i -dimensional parameterspace and where

$E_k(\underline{p} + \delta_i \hat{i})$ is the eigenenergy {corresponding to $E_k(\underline{p})$ of the Hamiltonian $H(\underline{p} + \delta_i \hat{i})$ to first order in δ_i

$$H(\underline{p} + \delta_i \hat{i}) \approx H(\underline{p}) + \frac{\partial H(\underline{p})}{\partial p_i} \delta_i \quad (\text{VI.15})$$

Using perturbation theory the eigenenergy can also be expressed to first order in δ_i

$$E_k(\underline{p} + \delta_i \hat{i}) = E_k(\underline{p}) + \langle k | \frac{\partial H}{\partial p_i} | k \rangle \delta_i \quad (\text{VI.16})$$

and consequently

$$\frac{\partial E_k}{\partial p_i} = \langle k | \frac{\partial H}{\partial p_i} | k \rangle \quad (\text{VI.17})$$

Similarly

$$\frac{\partial^2 E_k}{\partial p_i \partial p_i} = \lim_{\delta_i, \delta_j \rightarrow 0} \frac{E(\underline{p} + \delta_i \hat{i} + \delta_j \hat{j}) - E(\underline{p} + \delta_i \hat{i}) - E(\underline{p} + \delta_j \hat{j}) + E(\underline{p})}{\delta_i \delta_j} \quad (\text{VI.18})$$

Now to second order in δ 's

$$\begin{aligned} H(\underline{p} + \delta_i \hat{i} + \delta_j \hat{j}) &= H(\underline{p}) + \frac{\partial H}{\partial p_i} \delta_j + \frac{\partial^2 H}{\partial p_i \partial p_j} \delta_i \delta_j + \\ &+ \frac{\partial H}{\partial p_j} \delta_j + \frac{1}{2} \left(\frac{\partial^2 H}{\partial p_i^2} \delta_i^2 + \frac{\partial^2 H}{\partial p_j^2} \delta_j^2 \right) \\ &= H(\underline{p}) + V \end{aligned} \quad (\text{VI.19})$$

where V may be considered a small perturbation. As the parameters appear linearly in the Hamiltonian the last term goes to zero. By second order

perturbation, the eigenenergies are shifted to

$$E(\underline{p} + \delta_i \hat{i} + \delta_j \hat{j}) = E(\underline{p}) + \langle k|V|k\rangle + \sum_{l \neq k} \frac{\langle k|V|l\rangle \langle l|V|k\rangle}{E_k - E_l} \quad (\text{VI.20})$$

Thus

$$\frac{\partial^2 E}{\partial p_i \partial p_j} = \langle k | \frac{\partial^2 H}{\partial p_i \partial p_j} | k \rangle + 2 \sum_{l \neq k} \frac{\langle k | \frac{\partial H}{\partial p_i} | l \rangle \langle l | \frac{\partial H}{\partial p_i} | k \rangle}{E_k - E_l} \quad (\text{VI.21})$$

where the matrix elements $\langle k|M|l\rangle$ written in terms of the old basis are

$$\langle k|M|l\rangle = \sum_{\alpha, \beta} \langle k|\alpha\rangle \langle \alpha|M|\beta\rangle \langle \beta|l\rangle \quad (\text{VI.22})$$

The similarity transform is carried out by the subroutine STCM (see appendix D).

B. The Flow Chart

From the flow chart (see next page) the steps in the computational process can be followed. (Fig.VI.1.)

1. The input data is read in including all external parameters, initial estimates of the crystal parameters and the values of the tensor operator equivalents required. The input data after conversion is printed out.
2. The matrix elements that are independent of the field are calculated from the matrix in Table III.4 using the values for matrix elements given in Table III.7. (Main Programme, See Appendix A).
3. The remaining field dependent matrix elements are

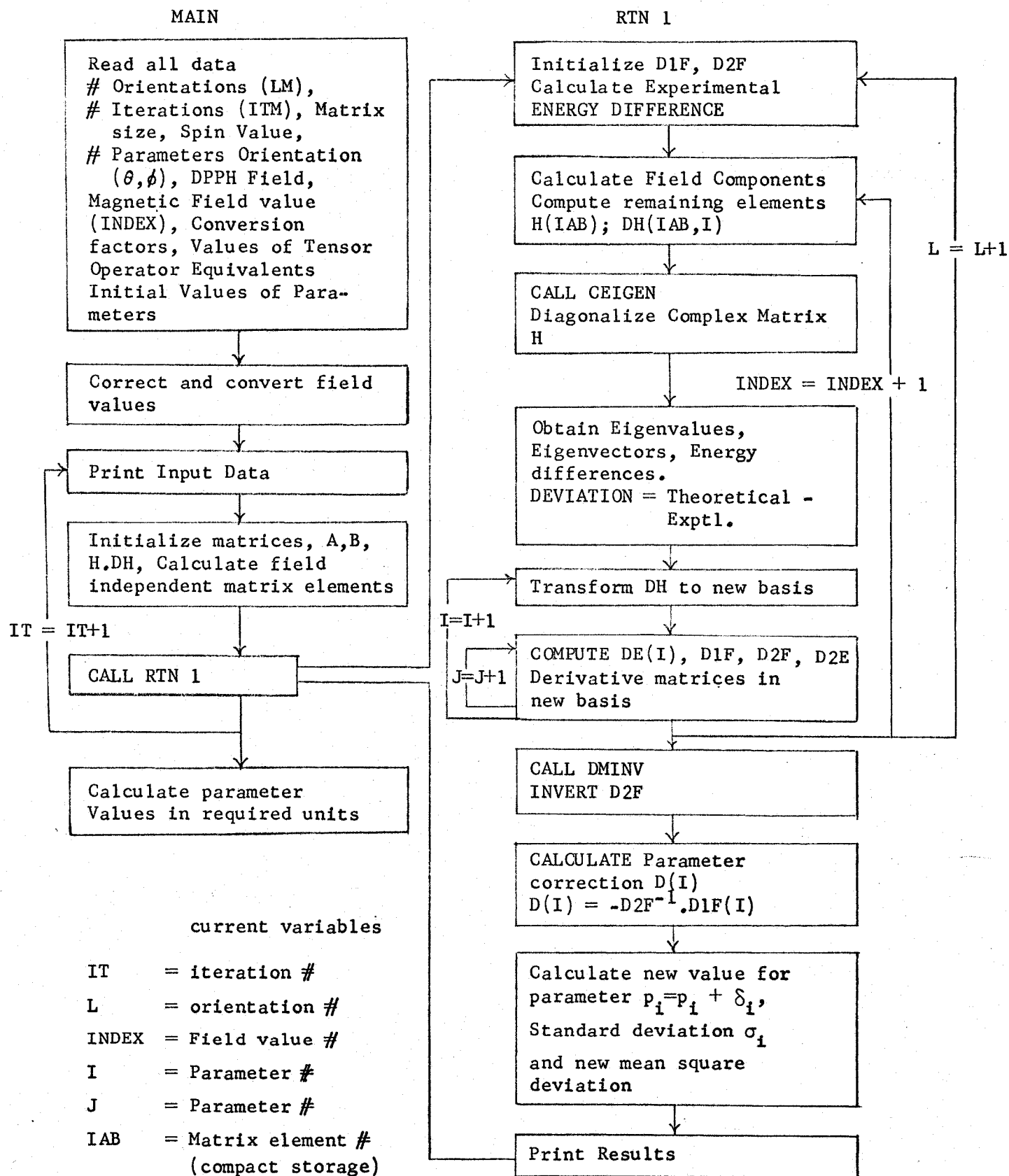


Fig VI.1. FLOW CHART FOR COMPUTER PROGRAMME

calculated using the components of the measured field values in addition to the data utilised in 2. (RTN 1 See Appendix B).

4. The Hamiltonian matrix formed in 2 and 3 is then diagonalised exactly using the subroutine CEIGEN (Appendix C) which returns eigenenergies and eigenvectors. The difference between the adjacent eigenvalues provides the basis of the least squares sum while the eigenvectors are used in the similarity transform in the next step. The value of DEVIATION printed out is a measure of the fit.
5. The derivative matrix is then transformed to the new basis in which the Hamiltonian is diagonal, see (VI.22). This then allows calculation of $DE(I)$, the derivative of the energy with respect to each parameter, see (VI.17) and the second derivative $D2E$, see (VI.21). From these the 1st and second derivatives of the least squares sum are formed, $D1F(I)$, see (VI.12) and $D2F$ see (VI.13).

Step 5 is repeated for each parameter in the $I = I+1$ loop, while the computation of the second derivatives is repeated for all parameters J , with each parameter I in the $J = J + 1$ loop.

Steps 3 to 5 are then repeated for each of the $(N-1)$ resonant fields at a given orientation during the $INDEX = INDEX + 1$ loop, which itself is repeated for each of the M orientations in the $L = L + 1$ loop.

6. As $D2F$ involves summation of both I and J simultaneously as well as a summation over all resonant fields it is not completed till the end of step 5. $D2F$ is then inverted using $DMINV$ (see Appendix E) The parameter correction $D(I)$ can then be calculated see (VI.11),

the new estimate of the parameters is then determined

$$P(I) = P(I) + D(I) \quad (VI.23)$$

The standard deviation for each parameter is then calculated together with an estimate of what the mean square deviation will be, using the new parameter values.

7. The results are printed and control returned to the main program where steps 2 to 7 are repeated for the number of iterations specified.
8. The parameters are converted to whatever units are required and any auxiliary calculations with the parameters may also be carried out here.

As a check on the inversion process and the reliability of the parameter values, the $D2F$ and $(D2F)^{-1}$ matrices are multiplied using the subroutine $DGMPRO$ (see Appendix F, based on IBM Routine $GMPROD$)²⁵ to see that the product is the unit matrix (see VI.11).

C. The Data Deck

The data cards incorporated in the program are described below.

Card 1:- Columns 1-5, integer right justified, number of orientations = LM.

This programme handles 12, MAIN is dimensioned to 16 but some arrays and formats will need to be redimensioned in RTN 1 and CEIGEN for LM > 12.

Columns 6-10, integer, right justified, number of iterations = ITM.

Card 2:- Columns 1-5, integer, right justified, size of matrix = N

(Degeneracy of ground state). Columns 6-10, floating point number,

spin value = . Columns 11-15, integer, right justified, number of parameters = IMAX.

Card 3:- Columns 1-80, User name or identification.

Card 4:- Columns 1-80, Description of Experiment.

Card 5:- Values of THETA for each orientation, Columns 1-5, 6-10, ..., 76-80.

Card 6:- Values of PHI as for 5.

Card 7:- Values for DPPH, MHz measured at poleface, columns 1-10, 11-20, ..., 71-80.

Card 8:- As for 7 when $8 < LM < 16$.

Card 9 - 20 (for 12 orientations):- Field values in MHz measured at poleface, entered 7 to a card, order determined as increasing magnitude on Z axis.

Each card represents one orientation, columns 1-10, 11-20, ..., 71-80.

Card 21:- Columns 1-10, 11-20, ..., 41-50.

Poleface correction = ADJ = 0.999934, Y-intercept = CADJ = 0.001436.

Corrects field at poleface to field at centre.

Conversion factor = PMHG = 0.234869. Converts proton frequency MHz to kg.

g value DPPH = GDP = 2.00360, g value free electron = GFE = 2.00229.

Cards 22-29 (Number varies):-

Matrix elements of the angular momentum tensor operators required.

Left justified floating point numbers in columns 1-10, 11-20, ..., 71-80.

(see Table III.6).

Card 30:- Estimated values of parameters in order shown in Format. Floating point numbers in columns 1-10, 11-20, ..., 71-80.

Card 31:- Remaining parameters or blank card.

D. Rate of Convergence

To indicate the rate of convergence a sample run is shown in Table VI.1, giving the mean square deviation in kgauss.

TABLE VI.1

| Iteration Number | Mean Square Deviation (kgauss) |
|---------------------|-----------------------------------|
| 1 | 0.9190 |
| 2 | 0.0220 |
| 3 | 0.0550 |
| 4 | 0.0022 |
| 5 | 0.0200 |
| 6 | 0.0006 |

Even though the value oscillates it can be seen that the convergence is quite rapid.

CHAPTER VII

RESULTS

When determining the position of the magnetic axes, turning points were found for each resonance line, the mean values and greatest deviation for each line are shown in Table VII.1.

TABLE VII.1

| LINE | Z-AXIS | | Y-AXIS | | -X-AXIS | |
|------|-------------------|--------------------|--------------------|---------------------|-------------------|--------------------|
| | θ_X | θ_H | θ_X | θ_H | θ_X | θ_H |
| I | 81.5 ± 0.1 | + 1.3 ± 0.0 | 351.4 ± 0.0 | - 0.7 ± 0.0 | 84.5 ± 0.1 | -87.8 ± 0.0 |
| II | 81.5 ± 0.0 | + 1.3 ± 0.1 | 351.4 ± 0.0 | - 0.7 ± 0.1 | 85.5 ± 0.5 | -89.9 ± 0.0 |
| III | 81.5 ± 0.1 | + 1.2 ± 0.1 | 351.1 ± 0.1 | - 0.7 ± 0.0 | 85.9 ± 0.1 | -90.7 ± 0.0 |
| IV | 81.4 ± 0.1 | + 1.1 ± 0.1 | 351.4 ± 0.0 | - 0.6 ± 0.2 | 86.0 ± 0.1 | -88.6 ± 0.0 |
| V | Saddle-point | | 351.4 ± 0.1 | - 0.6 ± 0.1 | 86.0 ± 0.2 | -89.2 ± 0.1 |
| VI | 81.6 ± 0.0 | + 1.2 ± 0.1 | 351.4 ± 0.1 | - 0.8 ± 0.2 | 85.3 ± 0.1 | -91.1 ± 0.2 |
| VII | 81.5 ± 0.1 | + 1.3 ± 0.1 | 351.4 ± 0.0 | Signal too small | 85.5 ± 0.5 | -89.9 ± 0.1 |

Means:

| | Z-Axis | Y-Axis | -X-Axis |
|--------------------|------------------|-------------------|------------------|
| $\bar{\theta}_X =$ | + 81.5 ± 0.1 | + 351.4 ± 0.3 | + 85.7 ± 1.2 |
| $\bar{\theta}_H =$ | + 1.2 ± 0.1 | - 0.7 ± 0.2 | - 89.6 ± 1.8 |

Error represents the maximum deviation over a series of readings.

As can be seen from the results, the Z and Y axes are well defined but the axis varies over 3° on the magnet scale. A similar variation in one axis of an angular variation plot is observed for gadolinium in a cubic field (Low^1). The fact that the X turning points occur at different orientations for each line leads to some uncertainty as to the exact position of the XY plane. This is overcome by using a plane perpendicular to the Z axis that passed through the well defined Y axis. This could lead to a 1° uncertainty for some orientations.

The results of the angular variation carried out in the XZ, YZ and XY planes may be seen plotted in Figs. VII.1, VII.2 and VII.3. Typical spectra with the field directed along each of the magnetic axes in turn are shown in Fig. VII.4, Z axis $[0001]$; Fig. VII.5a, X axis $[\bar{1}210]$; Fig VII.5b, Y axis $[101\bar{0}]$. The ratio of the line intensities for these spectra is shown in Table VII.2, where they have been normalised to the theoretical ratio which is also included (figures are given to the nearest integer).

TABLE VII.2.

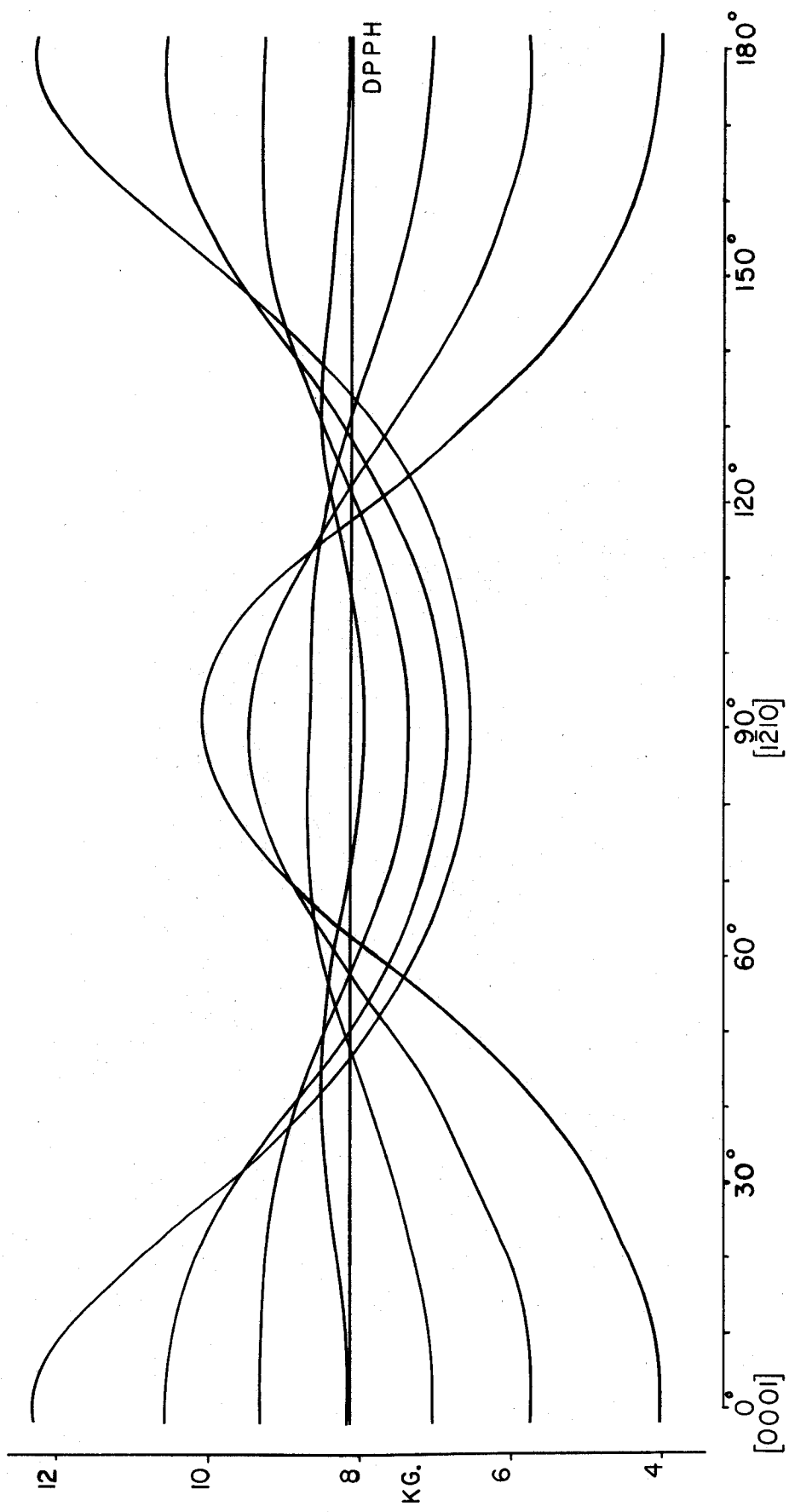
| | |
|-------------|--------------------------------|
| Theoretical | 7 : 12 : 15 : 16 : 15 : 12 : 7 |
| Z Axis | 4 : 8 : 12 : 16 : 12 : 10 : 5 |
| Y Axis | 2 : 6 : 11 : 16 : 11 : 7 : 4 |
| X Axis | 3 : 7 : 13 : 16 : 10 : 6 : 2 |

For calibration, fields measured at the poleface and the gap centre are recorded in Appendix G. A linear regression analysis was carried out on these values giving a correlation coefficient of 0.999999921 and a calibration curve of:

$$H_{\text{centre}} = 0.999934H_{\text{poleface}} + 0.001436 \quad (\text{VII.1})$$

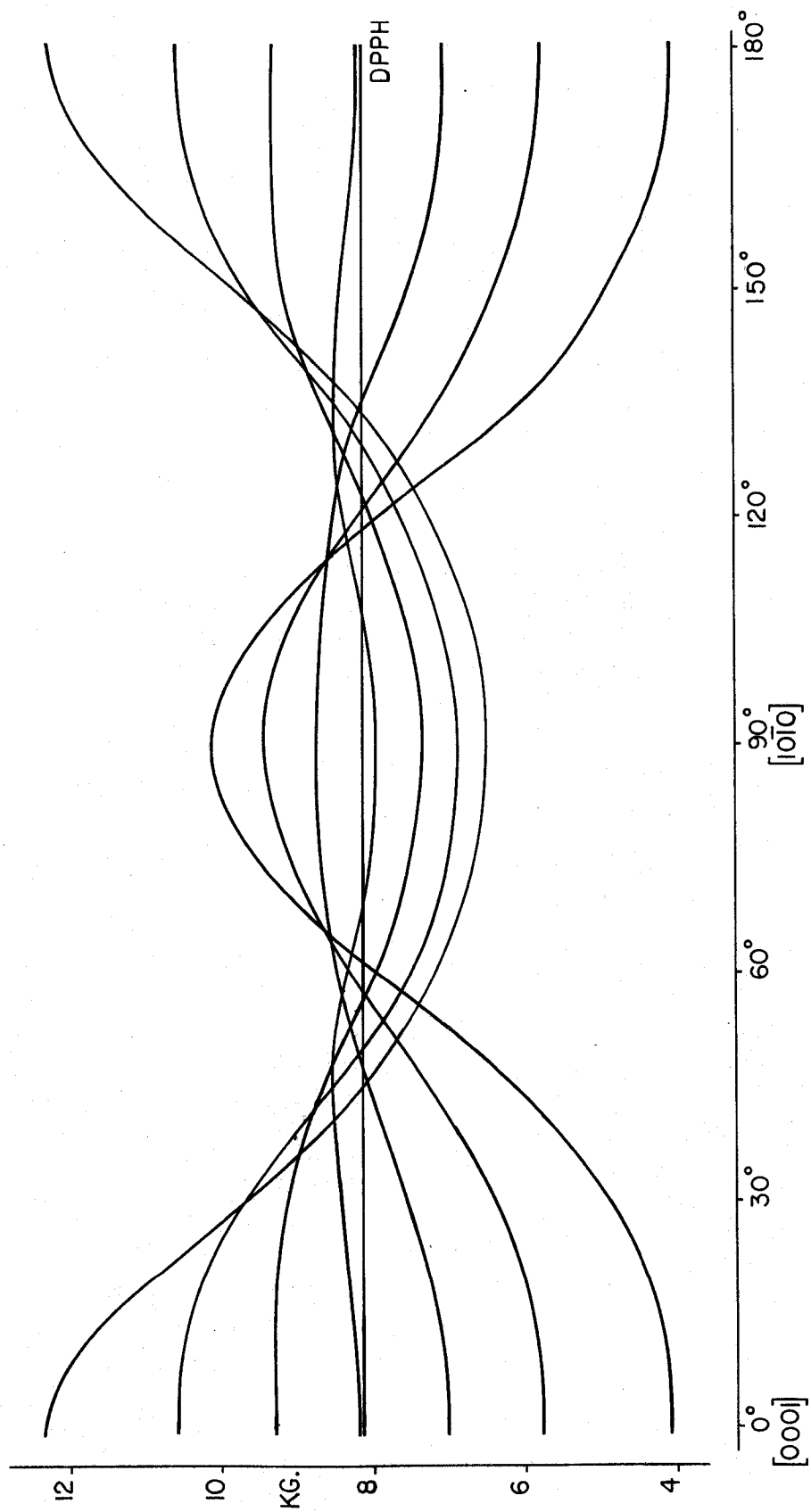
Proton Magnetometer readings for the resonant fields at a series of selected orientations, are given in Table VII.3. Using the calibration correction the field values have been converted to kilogauss and are presented in Table VII.4 together with the field value of DPPH used to measure the microwave frequency.

The values of the crystal field parameters calculated by the fitting programme are presented in Table VII.5 together with their standard deviations. The calculation was carried through sufficient iterations so that the change in the parameters, $D(I) = 0$, to 6 significant figures. In this case 4 iterations were required. A measure of the fit is given by the mean square deviation = 7.98×10^{-3} kg. which gives a R.M.S. deviation = 88 gauss for 63 resonant fields.



ANGULAR VARIATION IN XZ PLANE

Fig. VII.1.



ANGULAR VARIATION IN Z Y PLANE

Fig. VII 2

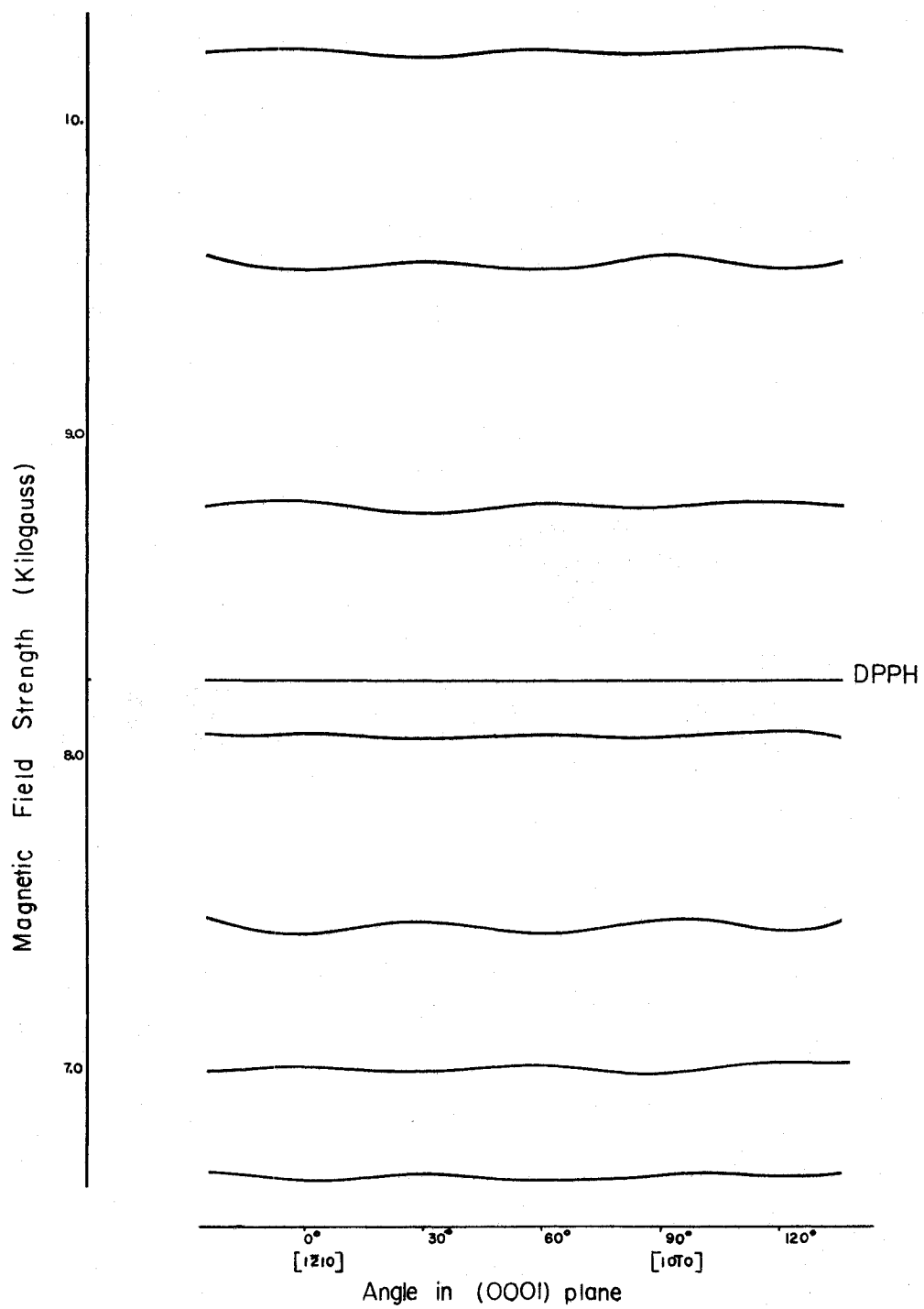


Fig. VII.3. ANGULAR VARIATION IN XY PLANE

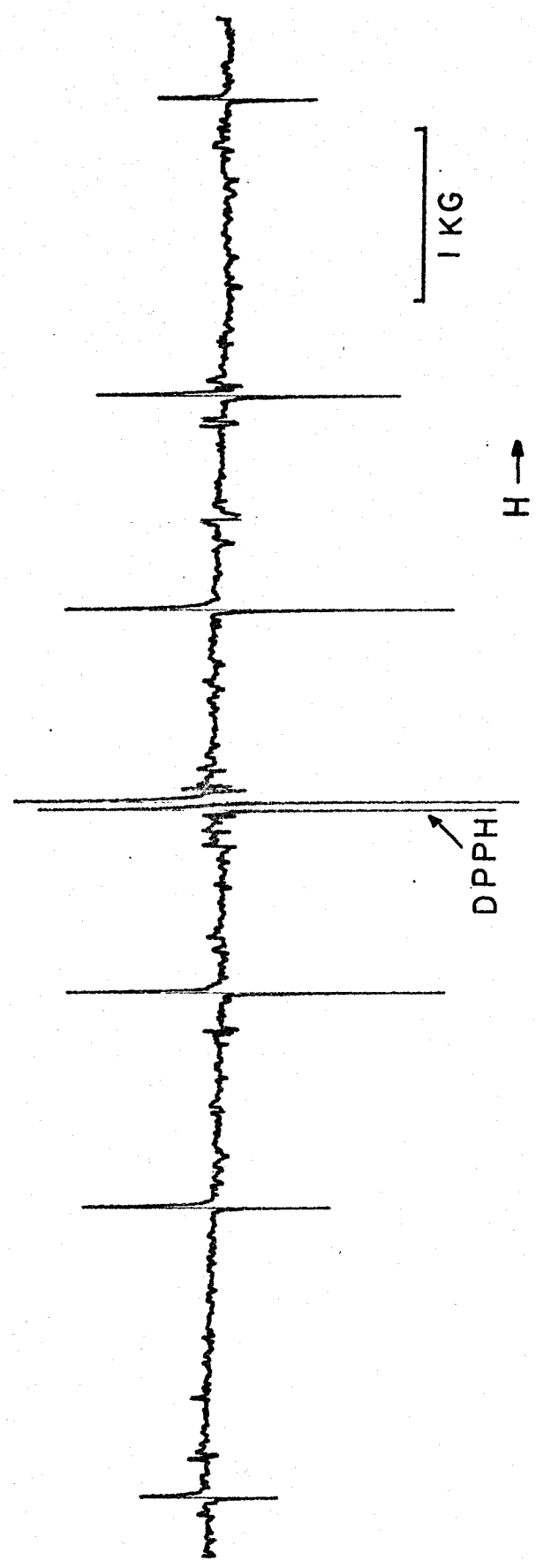


Fig VII.4 TYPICAL SPECTRUM WITH FIELD PARALLEL TO Z DIRECTION ALONG 0001 AXIS

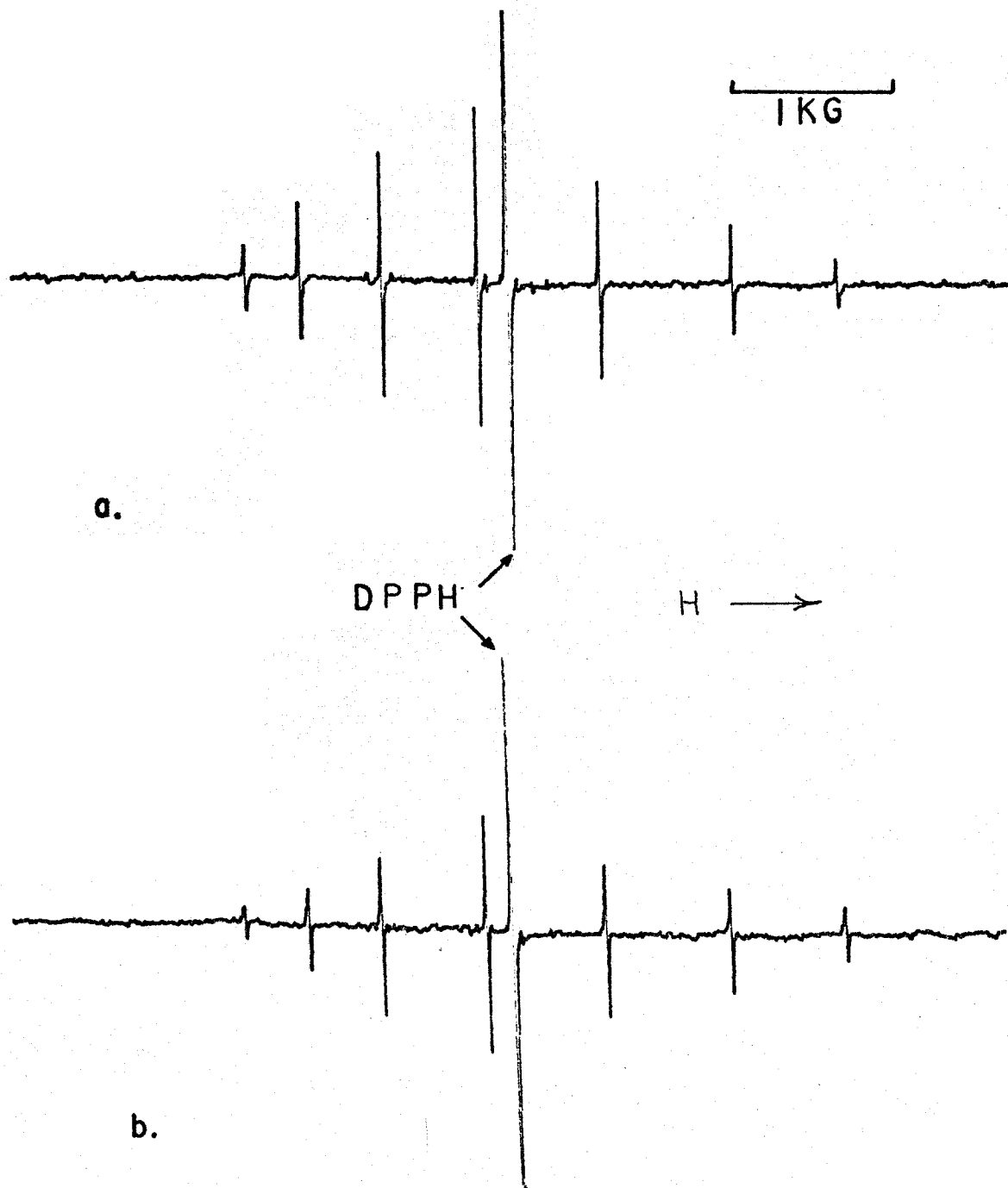


Fig VII 5. TYPICAL SPECTRUM IN DIRECTION PERPENDICULAR TO Z AXIS

a: ALONG $\bar{1}210$ DIRECTION

b: ALONG $10\bar{1}0$ DIRECTION

TABLE VII.3
PROTON MAGNETOMETER FREQUENCIES (MHz)

| Orientation | 1 | 2 | 3 | 4 | 5 | 6 | 7 | 8 | 9 |
|-------------|-----------------|-----------------|-----------------|-----------------|-----------------|-----------------|------------------|-----------------|-----------------|
| D.P.P.H. | 35.6104 ± 02 | 35.4821 ± 05 | 35.6126 ± 06 | 35.6207 ± 02 | 35.4850 ± 03 | 35.4966 ± 07 | 35.5005 ± 02 | 35.6090 ± 04 | 35.6146 ± 07 |
| θ | 0 | 90 | 90 | 180 | 90 | 70 | 110 | 71 | 109 |
| ϕ | 0 | 90 | 180 | 0 | 45 | 90 | 90 | 180 | 180 |
| Line I | 17.6950 ± 26 | 44.2855 ± 16 | 44.2891 ± 03 | 17.7120 ± 05 | 44.2542 ± 23 | 39.5481 ± 09 | 39.8836 ± 61 | 41.4346 ± 18 | 39.9501 ± 41 |
| II | 25.2823 ± 08 | 41.2347 ± 02 | 41.5487 ± 01 | 25.2944 ± 07 | 41.3294 ± 07 | 38.7770 ± 09 | 38.9431 ± 18 | 39.6242 ± 09 | 39.4626 ± 07 |
| III | 30.8824 ± 07 | 38.0060 ± 18 | 38.0333 ± 08 | 30.8949 ± 05 | 37.9579 ± 01 | 37.6495 ± 07 | 37.6844 ± 04 | 37.7864 ± 11 | 37.8568 ± 03 |
| IV | 35.8181 ± 03 | 34.7535 ± 09 | 35.8327 ± 05 | 34.8315 ± 13 | 35.7279 ± 07 | 35.7609 ± 10 | 35.7052 ± 13 | 35.5234 ± 12 | 35.7164 ± 05 |
| V | 40.7538 ± 02 | 31.9833 ± 05 | 32.2715 ± 04 | 40.7652 ± 03 | 32.0625 ± 05 | 33.4328 ± 14 | 33.3322 ± 06 | 33.2623 ± 09 | 33.4136 ± 04 |
| VI | 46.3503 ± 05 | 30.0876 ± 14 | 30.1023 ± 09 | 46.3610 ± 07 | 30.0395 ± 10 | 31.4862 ± 21 | 31.3851 ± 09 | 31.1551 ± 19 | 31.1828 ± 09 |
| VIII | 53.9340 ± 26 | 28.5000 ± 30 | 28.6804 ± 29 | 53.9344 ± 24 | 28.5351 ± 37 | 29.7891 ± 72 | 29.6985 ± 100 | 29.3322 ± 38 | 29.9654 ± 18 |

The error shown represents the maximum deviation over a series of readings.

| Orientation # | 1 | 2 | 3 | 4 | 5 | 6 | 7 | 8 | 9 |
|---------------|----------|----------|----------|----------|----------|---------|---------|---------|---------|
| D.P.P.H. | 8.36323 | 8.33310 | 8.36374 | 8.36565 | 8.33378 | 8.33650 | 8.33742 | 8.36290 | 8.36421 |
| θ | 0.0 | 90.0 | 90.0 | 180.0 | 90.0 | 70.0 | 110.0 | 71.0 | 109.0 |
| ϕ | 0.0 | 90.0 | 180.0 | 0.0 | 45.0 | 90.0 | 90.0 | 180.0 | 180.0 |
| Line I | 4.15607 | 10.40094 | 10.40179 | 4.16006 | 10.39359 | 9.28835 | 9.35732 | 9.73140 | 9.38276 |
| II | 5.93797 | 9.68445 | 9.75819 | 5.94082 | 9.70669 | 9.10725 | 9.14626 | 9.30622 | 9.26827 |
| III | 7.25318 | 8.92618 | 8.93259 | 7.25611 | 8.91488 | 8.84245 | 8.85065 | 8.87461 | 8.89114 |
| IV | 8.41234 | 8.16232 | 8.18094 | 8.41549 | 8.15631 | 8.39891 | 8.38557 | 8.34313 | 8.38846 |
| V | 9.57146 | 7.51173 | 7.57941 | 9.57419 | 7.53033 | 7.85215 | 7.82852 | 7.81203 | 7.84764 |
| VI | 10.88587 | 7.06652 | 7.06997 | 10.88838 | 7.05522 | 7.39498 | 7.37124 | 7.31722 | 7.32373 |
| VII | 12.66695 | 6.69366 | 6.73603 | 12.66702 | 6.70191 | 6.99679 | 6.97513 | 6.88911 | 7.03782 |

TABLE VII.4.

TABLE VII.5

CRYSTAL FIELD PARAMETERS

$$g_x = 1.990 \pm 0.005$$

$$g_y = 1.991 \pm 0.005$$

$$g_z = 1.989 \pm 0.006$$

| Parameter | Gauss | Standard deviation | Parameter | Units | |
|-----------------|--------|--------------------|-----------------------------|--------|-------------------------------|
| | | | | Gauss | (10^{-4} cm^{-1}) |
| B ₂₀ | -534.8 | 0.1 | b ₂ ⁰ | -655.0 | -0.6124 |
| B ₄₀ | -3.1 | 0.5 | b ₄ ⁰ | -11 | -0.011 |
| B ₆₀ | 0.2 | 0.1 | b ₆ ⁰ | +4 | +0.004 |
| B ₄₃ | 1.2 | 0.6 | b ₄ ³ | +27 | +0.03 |
| C ₄₃ | 0.7 | 0.6 | c ₄ ³ | +2 | +0.001 |
| B ₆₃ | -0.1 | 0.1 | b ₆ ³ | -170 | 0.2 |
| C ₆₃ | 0.1 | 0.1 | c ₆ ³ | +124 | 0.1 |
| B ₆₆ | -0.06 | 0.08 | b ₆ ⁶ | -9 | -0.009 |
| C ₆₆ | -0.05 | 0.16 | c ₆ ⁶ | -9 | -0.008 |

CHAPTER VIII

DISCUSSION AND CONCLUSION

After examining the data the most obvious point for discussion must be the poor fitting achieved with theoretically calculated energy levels (R.M.S. deviation = 88 gauss). The greatest deviation in the P.M.R. measurements of the resonant fields is ± 0.0100 in 29.6985 MHz measured on line 7 which, due to its low intensity, maintains the largest error throughout the experiment. This represents an error of 2.5 gauss or 0.03%. With the exception of the two end lines the error is, for the most part, less than 0.25 gauss. Considering this, together with some degree of misalignment of the crystal, it would not be unreasonable to expect the R.M.S. deviation of the fitting process to be < 5 gauss.

The R.M.S. error is then considerably greater than experimental error which would seem to indicate errors in measurement or orientation of the crystal. However, these data represent a second set of measurements which improved the R.M.S. error from 120 gauss to 88 gauss. As the second set of readings were taken on a different crystal, and the differences could be attributed to the method of defining the XY plane, it would seem that the measurements can be accepted as being accurate. The first set tried to define the XY plane by determining the turning points that occur every 30° (see Fig. VII.3), while the second method is described in chapters V and VII.

It would then appear that the model used in the theoretical calculations should be checked and may need some changes in the terms

included in the spin Hamiltonian. This can best be done by considering all of the information gathered from the system.

1. The fact that the Y axis is well defined and the X axis is not would appear to indicate an inequivalence of X and Y.

2. The angular variation in the YX plane is symmetric about the Y axis with collapse points spread over 35° but centred around 55° from the Z axis. The angular variation in the XZ plane however is not symmetric about the X axis and collapse points for pairs of lines occur up to 2° different on either side of the X axis, which is to be expected as an hydroxyl ion lies in the XZ plane on one side of the X axis but not on the other. This would seem to indicate an inequivalence of X and Y also. In the XY plane the angular variation shows a 60° periodicity which is probably associated with the B_{63} as it is the largest trigonal term. This periodicity causes the resonant fields to vary slightly in the X and Y directions up to 40 gauss for some lines (see VII.3).

3. If the behavior of the resonant fields is observed in a cone $\theta = 80^\circ$, 60° periodicity is noted. However, by the time $\theta = 70^\circ$ is reached the 60° periodicity disappears and is replaced by a 180° periodicity. A 180° periodicity was also observed for $\theta = 60^\circ$. A complete angular variation around one of these cones has not been made but 3 turning points have been noted 94° and 91° apart, the discrepancy from 90° probably is due to incorrect setting on the crystal rotator. Only a rough check has yet been made, varying the magnet scale but not the crystal.

The fact that a two-fold symmetry exists for the off-axis positions mentioned in 3, seems to suggest the need for the inclusion of some orthorhombic terms in the Hamiltonian, namely B_{22} , B_{42} and B_{44} .

The effect of these terms on the fitting is under investigation at present, and it is hoped that they will prove to be responsible for the present bad fit. Why these effects are found in gadolinium but not in manganese is probably due to the charge compensator associated with the Gd^{3+} ion causing local distortion of the site symmetry.

The intensity ratios in Table VII.2 show reasonable agreement with the theoretical, the fact that they are all below the theoretical values is probably due to increased line width.

The orthorhombic terms gave a fit with R.M.S. error of 91 gauss and so offered no improvement. For an orthorhombic distortion the charge compensator would have to be in a position off the z axis. With the three fold axis of symmetry associated with the site this would produce three sets of spectra due to the three inequivalent sites that the charge compensator could occupy.

The next stage in the investigation will involve the introduction of terms non-linear in magnetic field and also hyperfine and nuclear Zeeman terms.

BIBLIOGRAPHY

1. Low, W., Phys. Rev. 109, 265 (1958).
2. Jones, D.A., Baker, J.M. and Pope, D.F.D., Proc. Phys. Soc. 74, # 3, 249 (1959).
3. Marshall, S.A. and Serway, R.A., Phys. Rev. 171, # 2, 171 (1968).
4. Buckmaster, H.A., Chatterjee, R. and Shing, Y.H., J. Mag. Res. 4, 85 (1971).
5. Megaw, H.D., Proc. Roy. Soc. (London) A142, 198 (1933).
6. Bernal, J.D. and Megaw, H.D., Proc. Roy. Soc. (London) A151, 384 (1935).
7. Petch, H.E., Can. J. Phys. 35, 983 (1957).
8. Petch, H.E., Acta Cryst. 14, 950 (1961).
9. Busing, W.R. and Levy, H.A., J. Chem. Phys. 26, 563 (1957).
10. Henderson, D.M. and Gutowsky, H.S., Am. Mineral, 47, 1231 (1962).
11. Pelah, I., Krebs, K. and Imry, Y., J. Chem. Phys. 43, 1864 (1965).
12. Wyckoff, R.W.G., 'The Structure of Crystals', Vol. 2, (Reinhold Pub. Corp., N.Y., 1931).
13. Zavoyskiy, Ye. K. Zh. Eksp. Teor. Fiz. 17, 155 (1947).
14. Abragam, A. and Pryce, M.H.L., Proc. Roy. Soc. A205, 135 (1951).
15. Bleaney and Stevens, Reports on Progress in Physics XVI, 128 (1935).
16. Al'tshuler, S.A. and Kozyrev, B.M., 'Electron Paramagnetic Resonance', Academic Press, p.45 (1964).
17. Ibid, p.46.
18. Buckmaster, H.A., Chatterjee, R. and Shing, Y.H., J. Mag. Res. 4, 85 (1971).
19. Ibid, p.86.
20. Condon, E.V. and Shortley, G.H., 'The Theory of Atomic Spectra',

(Cambridge Univ. Press, 1951).

21. Holuj, F., Can. J. Phys. 46, 287 (1968).
22. Froberg, C.-E. 'Introduction to Numerical Analysis', Addison-Wesley, 1965, p.21.
23. Ibid, p.111.
24. IBM Publication 360A - CM, p.165.
25. Ibid, p.95.


```

      C      READ INITIAL VALUES OF PARAMETERS
      C
      C      READ ICS, (P(I), I=1, IMAX)
      C
      C      CORRECT AND CONVERT FIELD VALUES.
      C
      40      AP=ADJ*P/HR
      41      CAP=CADJ*P/HC
      42      DO 150 L=1, LR
      43      HOP(L)=HOP(L)*AF
      44      LIPD=L*7
      45      LIH=LIPD-6
      46      DO 150 INDEX=LIP, LIND
      47      HR(INDEX)=HR(INDEX)*AP+CAP
      48      150 CONTINUE
      49      PRINT 122, (HOP(L), L=1, LR)
      50      PRINT 121, (THETA(L), L=1, LR)
      51      PRINT 121, (PHI(L), L=1, LR)
      52      DO 143 J=1, 7
      53      143 PRINT 122, (HR(INDEX), INDEX=J, HR, 7)
      54      PRINT 123, ADJ, CADJ, PHFG, GDP, GPF
      55      DO 310 IT=1, IYM
      56      PRINT 130, IT
      57      PRINT 124
      C
      C      PRINT INITIAL PARAMETER VALUES.
      C
      68      PRINT 125, (P(I), I=1, IMAX)
      C      INITIALIZE MATRIX SET UP A(IAS), B(IAB)
      C
      70      DO 290 IAB=1, 36
      71      DO 291 I=1, IMAX
      72      291 B(IAB, I)=0.00
      73      B(IAB)=0.00
      74      A(IAB)=0.00
      75      290 P(IAB)=0.10
      76      DR2=DSQRT(2.00)
      77      DR=P
      78      IAB=1
      79      IB=2
      80      DO 300 K=1, NR
      81      A(IAB)=G02P08(K)*P(4)+G04P08(K)*P(5)+G06P08(K)*P(6)
      82      B(IAB)=G01P08(K)*P(3)
      83      DR(IAB, 4)=G02P08(K)
      84      DR(IAB, 5)=G04P08(K)
      85      DR(IAB, 6)=G06P08(K)
      86      IAB=IAB+IB
      87      300 IB=IB+1
      88      IAB=2
      89      IB=2
      90      NY=NR-1
      91      DO 301 K=1, NY
      92      A(IAB)=-P(1)*G01P1(K)/DR2
      93      B(IAB)=P(2)*G01P1(K)/DR2
      94      IAB=IAB+IB
      95      301 IB=IB+1
      96      IAB=7

```

```

001      Y = 1
002      CO = 1000
003      DO 303 N=1,NY
004          A(IAN) = G04P2(N)*P(7) + G04P3(N)*P(8)
005          B(IAN) = G04P2(N)*P(8) + G04P3(N)*P(10)
006          DV(IAN,7) = G04P2(N)
007          DV(IAN,8) = IPAN*(G04P2(N))
008          DV(IAN,9) = G04P2(N)
009          DV(IAN,10) = +IPAN*(G04P2(N))
010          IAN = IAN + 1
011      303  IB = IB + 1
012          IAN = 22
013          ID = 0
014          NY = 80 - 6
015          DO 304 K=1,NY
016              A(IAN) = G06P6(K)*P(11)
017              B(IAN) = G06P6(K)*P(12)
018              DV(IAN,11) = G06P6(K)
019              DV(IAN,12) = +IPAN*(G06P6(K))
020              IAN = IAN + 1
021      304  IB = IB + 1
022          CALL RTM1
023      310  CONTINUE
024          P(1) = P(1)*CFE
025          P(2) = P(2)*CFE
026          P(3) = P(3)*CFE
027          P(4) = P(4)*(1.5D0**0.5D0)
028          P(5) = P(5)*2.0D0*(10.0D0/7.0D0)**0.5D0
029          P(6) = P(6)*215.0D0/(231.0D0**0.5D0)
030          FT = 15.0D0*(2.0D0**0.5D0)
031          P(7) = P(7)*FT
032          P(8) = P(8)*FT
033          ST = 157.5D0*(5.0D0*11.0D0)**0.5D0
034          P(9) = P(9)*ST
035          P(10) = P(10)*ST
036          P(11) = P(11)*157.5D0
037          P(12) = P(12)*157.5D0
038          PRINT 220
039          PRINT 230,(P(I),I=1,6)
040          PRINT 231,(P(I),I=7,11,2)
041          PRINT 232,(P(I),I=8,12,2)
042          DO 630 I=4,IPAN
043      630  P(I) = P(I)*0.935D0
044          PRINT 235
045          PRINT 220,(P(I),I=1,6)
046          PRINT 231,(P(I),I=7,11,2)
047          PRINT 232,(P(I),I=8,12,2)
048          STOP
049          END

```

APPENDIX B


```

175     M(IAB,I)=I/DMAX(IAB,IBOIZ)
176     M(I,I)=I/DMAX(IAB,IBOIZ)
177     IAP=IAP+I
178     IAP=Z
179     DO 401 ID=3,NO
180     M(IAP)=M(IAB,BOUW)+M(IAP,BOUW)
181     IAC=IAP+I
182     IAP=Y
183     DO 402 ID=5,NO
184     M(IAP)=A(I/C)+I*AC*(B(IAB))
185     IAC=IAP+I
186     IAP=2Y
187     DO 404 ID=2,NO
188     M(IAB)=A(IAP)+I*AC*(B(IAB))
189     IAC=IAP+I
190     IAP=2Y
191     DO 404 ID=2,NO
192     M(IAB)=A(IAP)+I*AC*(B(IAB))
193     IAC=IAP+I
194     C
195     C           INITIALIZE MATRIX DM(IAB,,I) AND GET DC MATRIX
196     C           ELEMENTS OF DM/DP(I) I=1,IMAX
197     C
198     DC=1
199     IAC=1
200     IB=2
201     DO 401 K=1,NO
202     DM(IAB,1)=G01P0(K)*NZ
203     IAC=IAB+I
204     IAC=IB+1
205     IAB=2
206     IB=3
207     NY=NO-1
208     DO 425 K=1,NY
209     DM(IAB,1)=-G01P1(Y)*NY/DP2
210     DM(IAB,2)=I*AC*(G01P1(K)*NY/DP2)
211     IAB=IAB+I
212     IAB=IB+1
213     C           CALL CEIGEN DIAGONALIZE COMPLEX MATRIX M(IAB)
214     C           OBTAIN EIGEN VALUES STORED DIAGONALLY IN W(L,I)
215     C           OBTAIN EIGENVECTORS STORED IN EVECT(IE)
216     C
217     NV=0
218     CALL CEIGEN (M,EVECT,0,NV)
219     EV=1
220     IAP=1
221     J=2
222     DO 500 K=1,NO
223     FN(K)=M(IAB)
224     IAB=IAB+J
225     J=J+1
226     DO 502 K=2,NO
227     IA=K-1
228     FY(IA)=(FN(K)-FN(IA))
229     KP=((LOGEX)+(P-1))-LIND
230     E=EY(KP)
231     DELTA=E-F(L)
232     PSI(Y,204,DELTA)
233     C
234     C           TRANSFORM DM(IAB,I) TO NEW BASIS
235     C
236     LAP=DA=1
237     DO 504 L=1,2
238     IAB=1
239     DO 504 CALL STOP (OUT(IAB,I),DM(IAB,I),EVECT,0,NV,LAP,DA)

```

```

237      IAP=1
238      IAP=1
239      CALL STOR(DMT(IAP,1),DM(IAP,1),EVECT,4,DM,LA=DM)
240      LAMPA=3
241      DO 508 J=7,10
242      IAP=1
243      CALL STOR(DMT(IAP,1),DM(IAP,1),EVECT,4,DM,LA=DM)
244      LAMPA=6
245      DO 510 I=11,12
246      IAP=1
247      CALL STOR(DMT(IAP,1),DM(IAP,1),EVECT,4,DM,LA=DM)
248      LAMPA=2
249      DO 512 I=13,14
250      IAP=1
251      CALL STOR(DMT(IAP,1),DM(IAP,1),EVECT,4,DM,LA=DM)
252      LAMPA=4
253      I=15
254      IAP=1
255      CALL STOR(DMT(IAP,1),DM(IAP,1),EVECT,4,DM,LA=DM)
256      XLSP=XLSP+(DELTA**2)
257
258      C
259      C          SETTING UP DE(I)
260      C
261      KK=KM+1
262      KKV=(KM*KM+KK)/2
263      DO 520 I=1,IMAX
264      DE(I)=DM(KKV+IK,I)-DM(KK,I)
265
266      C
267      C          SETTING UP DE/DP(I) I=1,IMAX
268      C
269      DIF(I)=DIF(I)+(2*DELTA*DE(I))
270      CONTINUE
271
272      C
273      C          SETTING UP D2E/DP(I)DP(J)
274      C
275      DO 540 I=1,IMAX
276      DO 540 J=1,IMAX
277      IJ=1+(J-1)*IMAX
278      D2E=0.00
279      DO 529 ID=1,IM
280      IF(ID.LT.KM) GO TO 522
281      IF(ID.EQ.KM) GO TO 521
282      KID=KM+(ID*ID-ID)/2
283      DMTI=DCCDJG(DMT(KID,I))
284      DMTJ=DMT(KID,J)
285      IF(ID.EQ.KM) GO TO 533
286      521 IF(ID.LT.KM) GO TO 523
287      KIDA=KM+(ID*ID-ID)/2
288      DMTIA=DCCDJG(DMT(KIDA,I))
289      DMTJA=DMT(KIDA,J)
290      GO TO 525
291      522 KID=ID+(KM*KM-KM)/2
292      DMTI=DMT(KID,I)
293      DMTJ=DCCDJG(DMT(KID,J))
294      KIDA=ID+(KM*KM-KM)/2
295      DMTIA=DMT(KIDA,I)
296      DMTJA=DCCDJG(DMT(KIDA,J))
297      GO TO 525
298      523 KIDA=ID+(KM*KM-KM)/2
299      DMTIA=DMT(KIDA,I)

```

```

221      D2F=02F-2.00*DELTA*(U(I),J)
222      D2F=D2F+2.00*DELTA*DELTA/(E2(I)-E2(J))-2.00*DELTA*
223      D2F=D2F-2.00*DELTA*DELTA/(E2(I)-E2(J))
224      GO TO 535
225      D2F=D2F+2.00*DELTA*DELTA/(E2(I)-E2(J))-2.00*DELTA*DELTA/
226      1 (E2(K)-E2(L))
227      CONTINUE
228      D2F(IJ)=D2F(IJ)+(2.00*DELTA(I)*DELTA(J))-D2F*DELTA*
229      CONTINUE
230      NFREE=N-I*MAX
231      XLSF=XLSF/NFREE
232      DO 542 J=1,IMAX
233      D1F(I)=D1F(I)/NFREE
234      DO 542 J=1,IMAX
235      IJ=I+(J-1)*IMAX
236      D2F(IJ)=D2F(IJ)/NFREE
237      AD2F(IJ)=D2F(IJ)
238      542 CONTINUE
239      C
240      C           FIND PREDICTED DISPLACEMENTS D(I), CALCULATE NEW VALUES
241      C           FOR PARAMETERS P(I), PRINT RESULTS TOGETHER WITH
242      C           MEAN SQUARE DEVIATION FOR FITTING AND STANDARD DEVIATION
243      C           FOR EACH OF THE PARAMETERS
244      CALL DDIPV(D2F,IMAX,DETF)
245      DO 550 I=1,IMAX
246      IJ=1-IMAX
247      D(I)=0.00
248      DO 550 J=1,IMAX
249      IJ=IJ+IMAX
250      550 D(I)=D(I)-D2F(IJ)*D1F(J)
251      PRINT 200,(D(I),I=1,IMAX)
252      DO 560 I=1,IMAX
253      560 P(I)=P(I)+D(I)
254      PRINT 201
255      PRINT 225,(P(I),I=1,IMAX)
256      XLSMEV=XLSF
257      II=-IMAX
258      DO 600 I=1,IMAX
259      II=II+IMAX+1
260      XLSMEV=XLSMEV+D1F(I)*D(I)+(AD2F(II)*D(I)*D(II))/2.00
261      JMIN=I+1
262      IF(I.GE.IMAX) GO TO 600
263      DO 590 J=JMIN,IMAX
264      IJ=II-I+J
265      XLSMEV=XLSMEV+AD2F(IJ)*D(I)*D(J)
266      590 CONTINUE
267      600 CONTINUE
268      II=-IMAX
269      IF(D2F(II).LT.0.00) PRINT 205,I
270      DO 620 I=1,IMAX
271      II=II+IMAX+1
272      620 SIGMA(I)=DSQRT(DABS(D2F(II)*XLSMEV*2.00/NFREE))
273      PRINT 202,XLSF,XLSMEV
274      PRINT 203
275      PRINT 200,(SIGMA(I),I=1,IMAX)
276      RETURN
277      END
278      ADDIMP**  FORMAT STATEMENT      127 IS UNREFERENCED
279      ADDIMP**  FORMAT STATEMENT      210 IS UNREFERENCED

```

APPENDIX C

Subroutine: CEIGEN

Purpose: Compute eigenvalues and eigenvectors of a Hermitean matrix (double precision complex).

Usage: CALL CEIGEN (A, R, N, MV)

Description of parameters:

A - (COMPLEX * 16) original Hermitean matrix, destroyed during computation. Upon return, A is the diagonalized matrix with eigenvalues in ascending order on the diagonal. Compact storage is used, the upper right side of the matrix actually stored: the (I,J) element is the $I + (J * J - J)/2$ element of A for $I \leq J$. For $I > J$ the (I, J) element is the complex conjugate of the (J,I) element, i.e. of the $J + (I * I - I)/2$ member of A.

R - (COMPLEX *16) the unitary transformation which diagonalizes A. The columns of R are eigenvectors of A ordered as are the eigenvalues.

N - the order (dimension) of A and R

MV - input code:

0 compute eigenvalues and eigenvectors
 I compute eigenvalues only. (R need not be dimensioned but must still appear in calling sequence.)

Method: an extension of the Jacobi method to Hermitean matrices as given, for example in G.-E Froberg, Introduction to Numerical Analysis (Addison-Wesley, 1965) p. 111. The coding parallels that for EIGEN (see publication 360A-CM, p.165).

Programmed by: Wm. E. Baylis,
 Physics Department,
 University of Windsor.

Execution time: ~ 0.5 sec CPU on the IBM 360 Model 50 of University of Windsor for $N = 4$. The time will vary roughly as N^4 but will be less if some off-diagonal elements of A are initially = 0.

```

465      CALL DZGEBZ(1,5,0,0,0,CA,CR,0,0,MV)
C
C   COMPUTES DOUBLE PRECISION EIGENVALUES AND EIGENVECTORS (UNLESS MV=0)
C   OF THE HERMITEAN MATRIX CA OF DIMENSION M.
C   THE JACOBI METHOD IS USED.
C   EIGENVALUES ARE STORED IN THE DIAGONAL ELEMENTS OF CA IN ASCENDING
C   ORDER. THE EIGENVECTORS ARE STORED COLUMNWISE IN CR IN THE SAME
C   SEQUENCE.
C   W. E. BAYLIS. FEB 1972.
C
466      IMPLICIT REAL*8 (A,D,G,O-Z), COMPLEX*16(C)
467      COMPLEX*16 ONE/(1.000,0.000)/, ZERO/(0.000,0.000)/, DCONJG
468      REAL*8 COSP,COSP2,CDABS
469      DIMENSION CA(36),CR(64),CSINP(2)
C
C   CHECK DIMENSION
C
470      IF(M-1)1,2,5
471      1 PRINT 200,M
472      200 FORMAT(' ERROR. ATTEMPT TO DIMENSION CEIGEN BY M ',I6,'.1/1 STOP
      .EXECUTION. ')
473      STOP
474      2 IF(MV .EQ. 1) GO TO 4
475      CR(1) = ONE
476      4 RETURN
C
C   GENERATE IDENTITY MATRIX
C
477      5 RANGE = 1.00-12
478      IF(MV .EQ. 1) GO TO 25
479      IO = -M
480      DO 20 J=1,M
481      IO = IO + M
482      DO 20 I=1,M
483      IJ = IO + I
484      CR(IJ) = ZERO
485      IF(I .EQ. J) CR(IJ) = ONE
486      20 CONTINUE
C
C   COMPUTE INITIAL AND FINAL NORMS
C
487      25 ANORM = 0.000
488      Y = 0.000
489      IJ = 0
490      DO 35 J=1,M
491      DO 35 I=1,J
492      IJ = IJ + 1
493      X = CA(IJ)*DCONJG(CA(IJ))
494      ANORM = ANORM + X
495      IF(I .EQ. J) GO TO 35
496      Y = Y + X
497      35 CONTINUE
498      ANORM = 1.41400*DSORT(ANORM)
499      ANRMX = ANORM*RANGE/DFLOAT(M)
500      IF(Y .LE. ANRMX) GO TO 165
C
C   INITIALIZE INDICATORS AND COMPUTE THRESHOLD. THR
C
501      IND = 0
502      THR = ANORM
503      45 THR = THR/DFLOAT(M)

```

```

505      L = (L+1)/2
506      LL = L-1
507      LL = LL + 1
508      LL = LL - 1
509      LL = (LL+1)/2
510      L = L + *P
C
C   COMPUTE ELEMENTS OF CYZ ROTATION MATRIX IF CON-TO-CON-ANGLE IS
C   LARGER THAN TWO
C
511      GAN = GANS(C*(L**))
512      IF(GAN .LT. TWO) GO TO 130
513      P = PD + 1
514      LD = P*(P-1)
515      PD = 1
516      X = CA(LD)
517      IF(X .LT. 0.000) GAN = -GAN
518      X = (CA(LL) - CA(PD))/2.000
519      Y = GAN/DSQRT(X**2+GAN**2)
520      IF(X .LT. 0.000) Y = -Y
521      SINTP = Y/DSQRT(2.000*(1.000 + DSQRT(1.000 - Y**2)))
522      SINTP2 = SINTP*SINTP
523      COSP2 = 1.000 - SINTP2
524      COSP = DSQRT(COSP2)
525      CSINTP(1) = GAN*SINTP/CA(LD)
526      CSINTP(2) = DCONJG(CSINTP(1))
527      CSINTP2 = 2.000*GAN*SINTP*COSP
C
C   RESTORE COLUMNS AND ROWS I AND K
C
528      ID = 0
529      DO 125 I=1,N
530      ID = ID + I - 1
531      IF(I-0) 85,115,90
532      85 ID = I + *Q
533      RCONJ = 1
534      IF(I-L) 100,115,105
535      100 IL = I + LG
536      LCONJ = 1
537      GO TO 110
538      90 ID = *R + ID
539      RCONJ = 2
540      105 IL = L + ID
541      LCONJ = 2
542      110 CX = CA(ID)*CSINTP(RCONJ)
543      CY = CA(IL)*CSINTP(3-LCONJ)
544      IF(RCONJ .EQ. LCONJ) GO TO 112
545      CA(IL) = CA(IL)*COSP + DCONJG(CX)
546      CA(ID) = CA(ID)*COSP - DCONJG(CY)
547      GO TO 115
548      112 CA(IL) = CA(IL)*COSP + CY
549      CA(ID) = CA(ID)*COSP - CX
550      115 IF(PV .EQ. 1) GO TO 125
551      IIP = ILO + I
552      IPK = IPQ + I
553      CX = CR(ILR)*COSP + CR(IPR)*CSINTP(1)
554      CR(IPR) = CR(IPR)*COSP - CR(ILR)*CSINTP(2)
555      CR(ILR) = CX
556      125 CRPT)=0F
557      X = CA(LL)*SINTP2 + CA(PD)*COSP2 - (C*)**2

```



```

C      COMPUTE STIFFNESS MATRIX FROM DATA OF POINTS
C      DISPLAY STIFFNESS MATRIX FROM POINTS, NUMBER OF POINTS
C      IN DATA FILE AND FILE
C
424      CCM=LEXY*II- /S(38),S(37),T(64),ZERR,DOO,IG
425      DATA ZERR/(0.00,0.00)/
426      DO 1 IJ=1,36
427      * AP(IJ)=ZERO
428      * LAMP1=LAMBDA+1
429      * K=K+1
430      DO 20 I=KH,HI
431      * C=15 J=1,6
432      * IJ=I+(J*J-J)/2
433      * IF(I.GT.J) IJ=J+(I*I-I)/2
434      * AP(IJ)=ZERO
435      DO 10 C=LAMP1,4
436      * L=K-LAMP1
437      * LK=L+(K*K-K)/2
438      * LI=L+(I-I)*N
439      * KJ=K+(J-1)*N
440      * KI=LI+K-L
441      * LJ=KJ+L-K
442      10 AP(IJ)=DCONJG(T(LI))*A(LK)*T(KJ)+T(LJ)*DCONJG(A(LI)*T(LI))+DTC
443      * IF(I.GT.J) AP(IJ)=DCONJG(AP(IJ))
444      * IF(LAMP1.EQ.0) AP(IJ)=AP(IJ)/2.00
445      15 CONTINUE
446      20 CONTINUE
447      DO 30 J=1,6
448      * I=J
449      * IJ=I+(J*J-J)/2
450      * AP(IJ)=ZERO
451      DO 25 K=LAMP1,4
452      * L=K-LAMBDA
453      * LK=L+(K*K-K)/2
454      * LI=L+(I-I)*N
455      * KJ=K+(J-1)*N
456      * KI=LI+K-L
457      * LJ=KJ+L-I
458      25 AP(IJ)=DCONJG(T(LI))*A(LK)*T(KJ)+T(LJ)*DCONJG(A(LI)*T(LI))+DTC
459      * IF(LAMBDA.EQ.0) AP(IJ)=AP(IJ)/2.00
460      30 CONTINUE
461      * RETURN
462      * END
463

```



```

216      A(I+1) = A(I) - A(I)
217      C I = K + 1
218      A(IK) = A(IK)/(1 - PIV)
219      55 CONTINUE
220      C
221      C     PIVOT MATRIX
222      C
223      60 65 I=1,N
224      IK=IM+I
225      POLD = A(IK)
226      IJ=Y-M
227      60 65 J=1,M
228      IJ=IJ+1
229      IF(I-K) 60,68,60
230      60 IF(J-K) 62,65,62
231      62 KJ=IJ+K-I
232      A(IJ) = POLD*A(KJ)+A(IJ)
233      65 CONTINUE
234      C
235      C     DIVIDE PIV BY PIVOT
236      C
237      70 KJ=K-M
238      70 75 J=1,M
239      KJ = KJ + M
240      IF(J-K) 70,78,70
241      70 A(KJ) = A(KJ)/PIVA
242      75 CONTINUE
243      C
244      C     PRODUCT OF PIVOTS
245      C
246      C     REPLACE PIVOT BY RECIPROCAL
247      C
248      80 A(KK) = 1.000/PIVA
249      80 CONTINUE
250      C
251      C     FINAL ROW AND COLUMN INTERCHANGE
252      C
253      90 K = N
254      100 K = K - 1
255      101 IF(K) 150,150,105
256      105 I=L(K)
257      106 IF(I-K) 120,120,109
258      109 J0 = K*(K-1)
259      110 J1 = I*(I-1)
260      60 110 J=1,N
261      JK = J0+J
262      HOLD = A(JK)
263      JI = J1+J
264      A(KK) = -A(JI)
265      110 A(JI) = HOLD
266      120 J=L(K)
267      121 IF(J-K) 101,100,125
268      125 KI=K-N
269      60 130 I=1,M
270      YI=KI+K
271      HOLD=A(YI)
272      JI = KI - K + J
273      A(KI) = -A(JI)
274      130 A(JI) = HOLD
275      60 TO 100

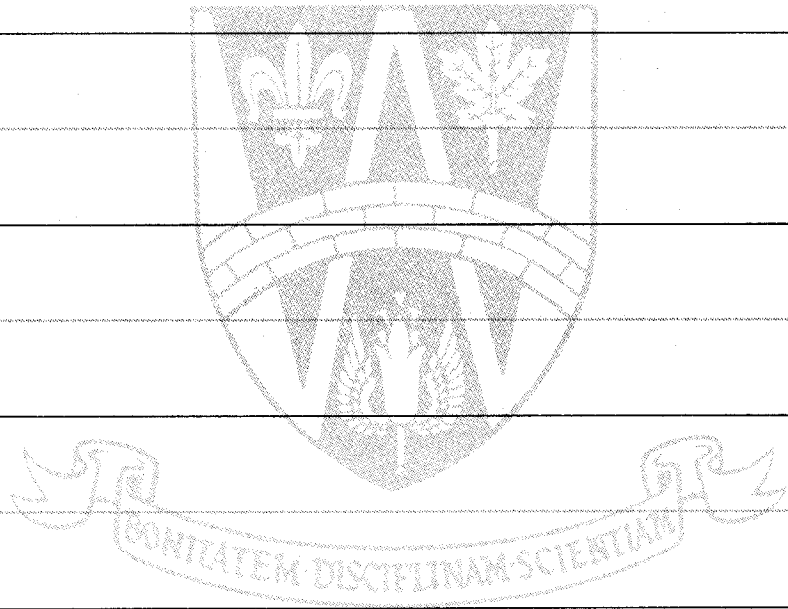
```

```

421
422
423
424

```

```
1  DIMENSION A(144),B(144),C(144)
2  IMPLICIT REAL*8(A-Z)
3  DIMENSION A(144),B(144),C(144)
4  IR=0.00
5  IK=-6
6  DO 10 K=1,1
7  IK=IK+6
8  DO 10 J=1,8
9  IR=IR+1
10  JJ=J-6
11  IR=IK
12  R(IR)=0.00
13  DO 10 I=1,8
14  JJ=JJ+6
15  IR=IR+1
16  R(IR)=R(IR)+A(JJ)*B(IR)
17  RETURN
18  END
```



APPENDIX G

| Nominal Field in KG | Pole Face MHz | Centre MHz | Difference MHz |
|------------------------|------------------|---------------|-------------------|
| 4.5 | 19.4761 | 19.4754 | 0.0007 |
| 6.0 | 25.9100 | 25.9087 | 0.0013 |
| 7.0 | 30.1988 | 30.1975 | 0.0013 |
| 8.0 | 34.4924 | 34.4913 | 0.0011 |
| 9.0 | 38.7812 | 34.7792 | 0.0020 |
| 10.0 | 43.0726 | 43.0707 | 0.0019 |
| 11.0 | 47.3530 | 47.3503 | 0.0027 |
| 12.0 | 51.6332 | 51.6308 | 0.0024 |

VITA AUCTORIS

I was born in Belmont, N.S.W., Australia, in 1945, completed Primary Education at Swansea Public School, 1956 and Secondary Education at Belmont High School, 1961. My B.Sc. in Physics was obtained from Newcastle University College in 1964 and my Diploma in Education in 1965. I taught Physics at Wollongong High School, Wollongong, from 1966 - 68 and at Swansea High School during 1969. I taught at W.F. Herman Collegiate, Windsor, Ontario, from 1969 until 1971 and I am at present completing requirements towards my M.Sc. degree at the University of Windsor, Ontario.